SPACE SYSTEMS

GE-SSO-69SD4282
JUNE 12,1969

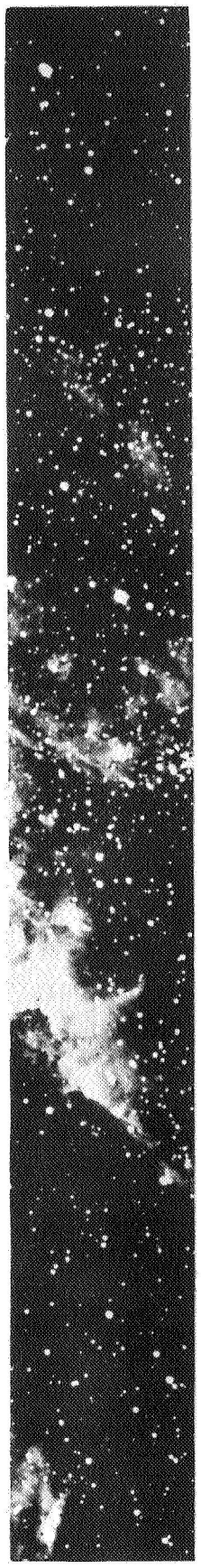

QUARTERLY REPORT NO.1
ROLLUP SUBSOLAR ARRAY

Prepared for: Jet Propulsion Laboratory

Prepared Under: Contract 952314

Edited by:

K. Hanson

GENERAL ELECTRIC

DOCUMENT NO. 69SD4282
JUNE 12, 1969

ROLLUP SUBSOLAR ARRAY

QUARTERLY TECHNICAL REPORT NO. 1

5 MARCH 1969 TO MAY 30, 1969

PREPARED FOR:

JET PROPULSION LABORATORY
CALIFORNIA INSTITUTE OF TECHNOLOGY
4800 OAK GROVE DRIVE
PASADENA, CALIFORNIA

PREPARED UNDER: CONTRACT 952314
CONTRACTING OFFICER: E.C. FLARITY
PROJECT MANAGER: W.A. HASBACH

PREPARED BY:

K.L. HANSON, EDITOR
F. BLAKE
N. LURIA
R. KYLE
R. FERGUSON
R. CARMICHAEL

APPROVED BY:

K L Hanson

K.L. HANSON,
PROJECT MGR.

THIS WORK WAS PERFORMED FOR THE JET PROPULSION LABORATORY, CALIFORNIA INSTITUTE OF TECHNOLOGY, AS SPONSORED BY THE NATIONAL AERONAUTICS AND SPACE ADMINISTRATION UNDER CONTRACT NAS 7—100

GENERAL ELECTRIC

SPACE SYSTEMS ORGANIZATION
Valley Forge Space Center
P. O. Box 8555 • Philadelphia, Penna. 19101

"This report contains information prepared by the General Electric Co., Space Systems Organization, under JPL Subcontract. Its content is not necessarily endorsed by the Jet Propulsion Laboratory, California Institute of Technology, or the National Aeronautics and Space Administration."

TABLE OF CONTENTS

LIST OF ILLUSTRATIONS

LIST OF TABLES

ABSTRACT

Results of the activities performed during the first quarter of the project to design and develop the technology of a 30-watt per pound rollup solar array are reported. These include the analysis of the effects of the stowed vibration, of the dynamic loads used in the feasibility design, bearing and lubrication selection, electrical performance, results of thermal cycling of segments of the array blanket, and work to date on analytical modeling of the system in the stowed and deployed configuration. The system design concept is described and activities planned for the next quarter are listed.

SECTION 1
INTRODUCTION AND SUMMARY

A program to generate a detailed design, fabricate, assemble and test a 250 square foot rollup subsolar array, capable of providing a minimum of 30 watts of electrical power per pound of subsolar array weight, was initiated March 5, 1969. The term subsolar array is used to indicate that although the item being designed is a complete solar array with respect to spacecraft application the item is one unit of solar array system that utilizes four identical units to provide the electrical power requirements for an interplanetary spacecraft design concept. The subsolar array is a complete subsystem, and the design requirements are intended to provide a technology for other mission applications. An extensive environmental test program is planned to establish the integrity of the design for spacecraft applications; to provide performance data; and to verify analysis techniques that will have application to large-area lightweight solar array designs based on the rollup concept.

The design of the rollup subsolar array is based on the concepts and technology developed in the Feasibility Study for a 30 Watts per Pound Rollup Solar Array (JPL Contract 951970) and was documented in Reference 1. For convenience, the 250 square foot rollup subsolar array unit will be referred to in this and subsequent reports as the RA250.

This First Quarterly Report describes the technical results achieved through May 31, 1969. The initial task was to establish a detailed program plan for the 15-month effort. Early in the program, emphasis was placed on the completion of the analysis and detail design of the RA250 to allow hardware fabrication to proceed. Design of the support equipment, detailed test planning, and analysis of the deployed dynamics of the system are being started in an orderly manner. The overall project schedule is shown in Figure 1-1.

The stowed vibration environment increased from the levels of the Feasibility Study and early analytical efforts included the investigation of the effects on weight and design selections. Some weight increase is anticipated and it is expected the design concept for some of the structural elements; e.g., the drum center support, and end supports will change. An analytical model is being exercised to provide the dynamic loads for stress analysis.

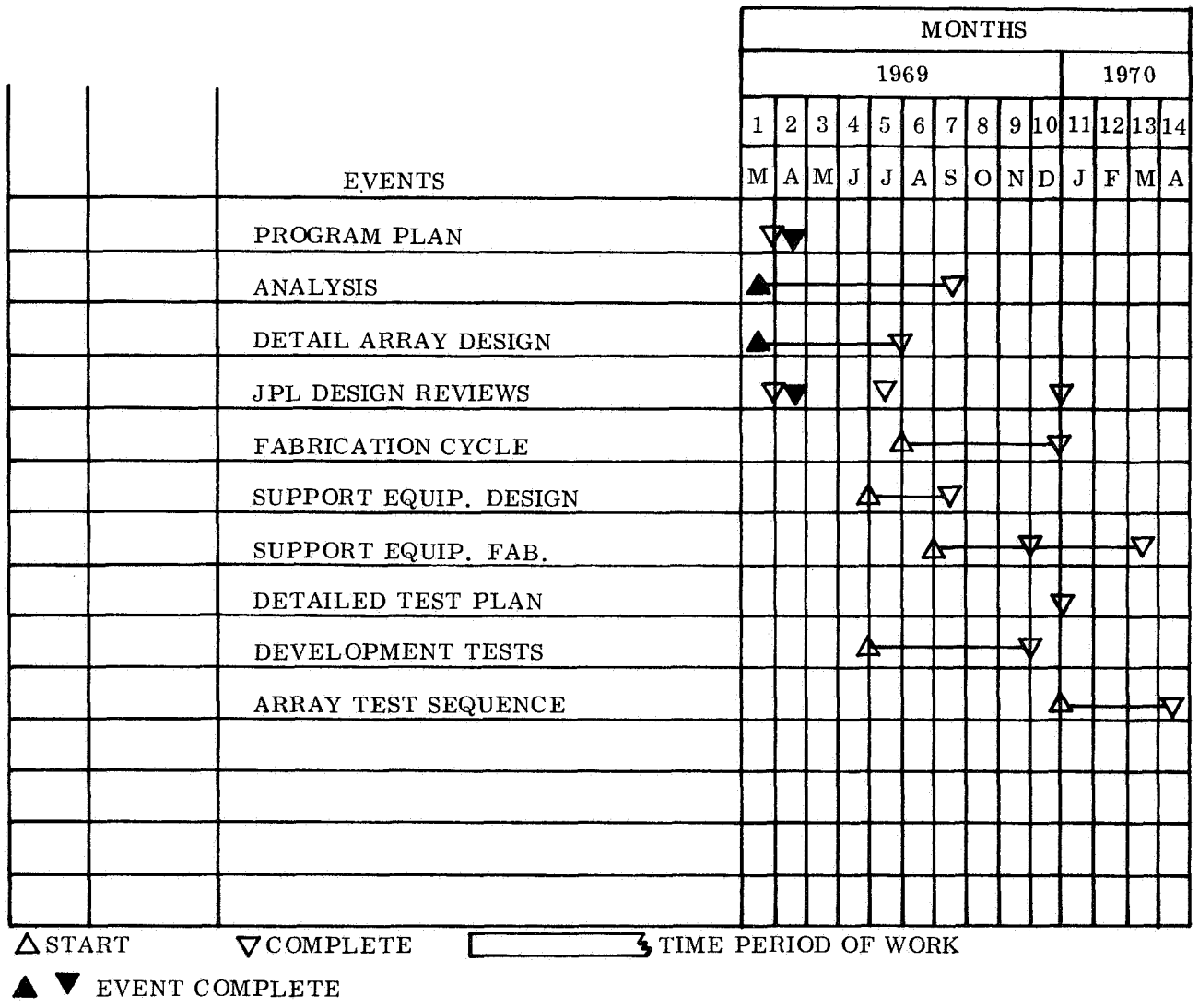

Figure 1-1. Master Program Schedule

The electrical performance of the system is described and shows that the maximum power is 2523 watts at 102 volts. A "worst case" analysis of the "Hot Spot" solar array heating phenomena is presented; it is concluded that no special design precautions are needed to protect this array from this type failure.

Bearing selections are discussed with the selected lubricant being RT-Duroid 5813. An analysis of the spring motor requirements is presented and the results of thermal cycling tests on solar array segments are tabulated. Key performance parameters for the solar panel actuator and the slip ring assemblies were excerpted from the component specifications and included in this report.

Present estimates of the increased structure weight due to the increased dynamic loads is 3 pounds; the weight allowance for the solar panel actuator has increased 1 pound. At the present estimated total weight, the specific performance is 31.1 watts per pound.

The results of an analysis of the solar array blanket treating it as a continuum are presented. This effort is directed toward an anlytical model of the deployed system where the blanket represents an unusual structural element and is a major fraction of the total system weight. Thus, it is an important part of the total analytical model.

The status of the development of manufacturing processes for the solar array blanket are described.

SECTION 2

TECHNICAL DISCUSSION

2.1 DESIGN REQUIREMENTS SUMMARY

2.1.1 INTRODUCTION

The RA250 rollup subsolar array shall provide 250 square feet of solar cell area with a minimum performance goal of 30 watts of electrical power per pound of system weight, under space illumination conditions at one Astronomical Unit (AU) and at an array temperature of 55°C. The subsolar array is to be one unit of a four-unit system that is compatible with an interplanetary spacecraft concept whose nose fairing and spacecraft envelope is defined in Figure 2-1.

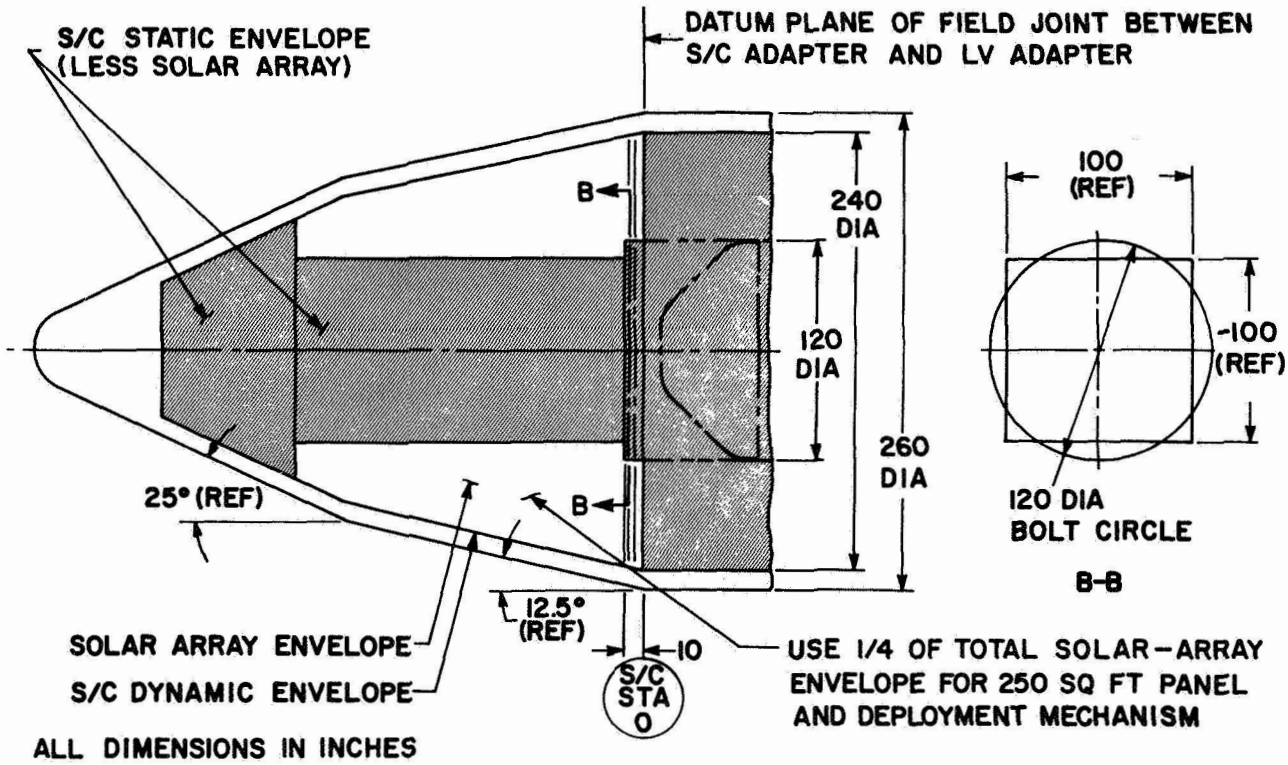

Figure 2-1. Nose Fairing and Spacecraft Envelope

A nominal power output of 10 watts per square foot at air mass zero, 1 AU solar illumination at 55°C has been specified, and power to weight ratio calculations are based on this performance. Analysis shows this to be within the state of the art of the nominal 8 mil silicon solar cells and the arrangement being used on the RA250. The performance translates to a weight goal of 83.3 pounds for the complete system.

Solar cell wiring, interconnecting, and structural techniques will be designed to minimize the magnetic field produced by the flow of current in the subsolar array.

2.1.2 LAUNCH ENVIRONMENT*

The design of the RA250 in the launch (stowed) configuration is to be based upon the following environment:

2.1.2.1 Vibration

2.1.2.1.1 Sinusoidal Vibration

The sinusoidal vibration input levels at frequencies between 10 and 2000 Hz are specified in Table 2-1. These levels are specified at the interface between the subsolar array assembly and the spacecraft. The sinusoidal vibration sweep rate shall be 1.0 octave/minute, along each of three mutually perpendicular axes; one of which shall be in the array deployment direction, and another shall be parallel to the rollup drum axes.

Table 2-1. Sinusoidal Vibration

Frequency Range (Hz)	Input Level	Sweep Rate (Oct/Min)
5 - 10	0.900 inch double displacement	1.0
10 - 225	4.6 G's peak	
225 - 550	0.00176 inch double displacement	
550 - 2000	27 G's peak	

Note: See Figure 2-2 for sinusoidal vibration plot.

*Reference 2 is the Detailed Specification for the RA250 Design Requirements.

2.1.2.1.2 Random Vibration

Specified as a shaped spectrum of random vibration defined by Table 2-2. The vibration shall be of Gaussian amplitude distribution except that instantaneous peak amplitudes of greater than 3 sigma shall be suppressed. For each of the three axes defined for sinusoidal vibrations the full vibration level shall be maintained for the duration of 60 seconds. Vibration levels are specified at the same assembly/spacecraft interface defined for sinusoidal vibration.

Table 2-2. Random Vibration

Frequency Range (Hz)	Power Spectral Density (G^2/Hz)	Wide Band rms (G level)
90 - 700	1.0	
20 - 90	Increasing at 6 db/oct	33.0
700 - 2000	Decreasing at 6 db/oct	

Note: See Figure 2-3 for random vibration noise plot.

2.1.2.2 Acoustic

The launch acoustics environment is specified as 60 seconds of random incidence, reverberant sound field, having the third-octave band sound pressure levels defined in Table 2-3.

Table 2-3 also defines the third-octave band sound pressure allowable tolerances. Below 80 Hz, the spectrum shall be rolled off at the rate of 24 db/octave or greater. Above 10,000 Hz, the sound pressure level in any one-third octave band shall not exceed 99 db reference to 0.0002 dynes/cm^2.

The overall sound pressure level for the spectrum given in Table 2-3 is approximately 150 db reference to 0.0002 dynes/cm^2; however, the spectral levels within each one-third octave band defines the basic requirements.

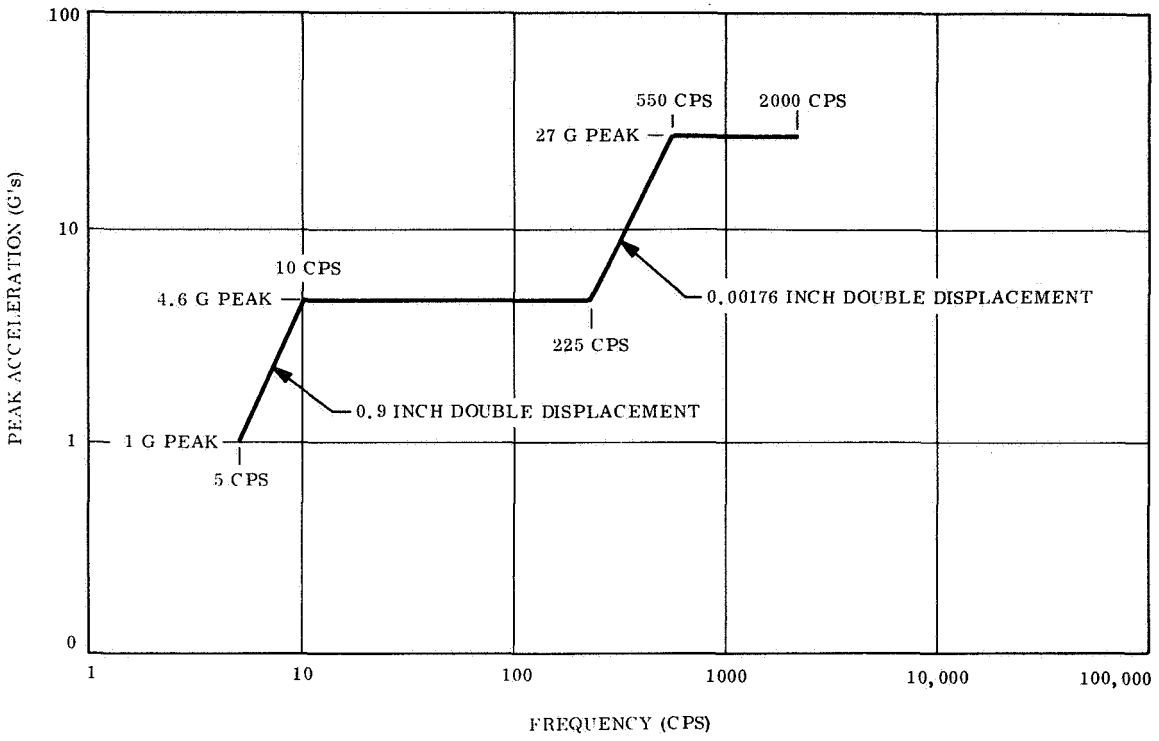

Figure 2-2. Sinusoidal Vibration

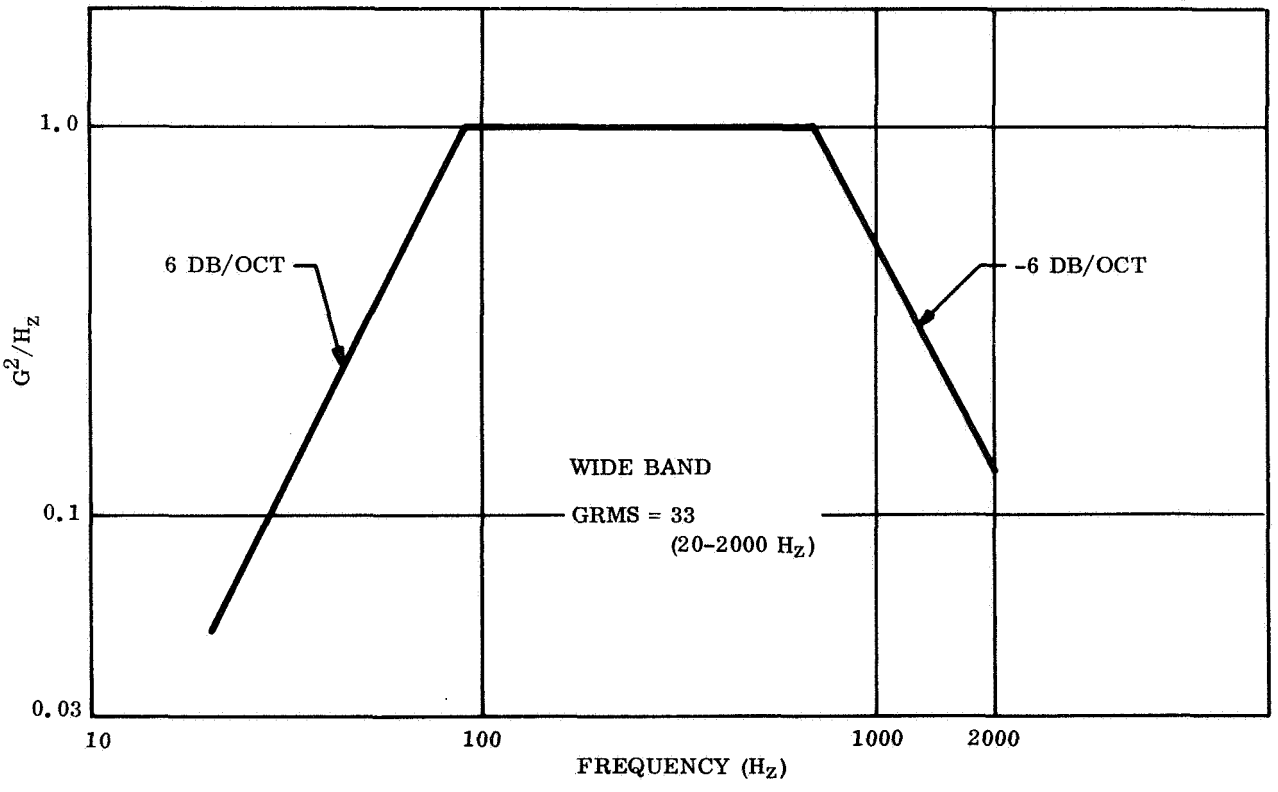

Figure 2-3. Random Vibration Noise Plot

Table 2-3. Acoustic Test Levels

1/3 Octave Band Center Frequency (cps)	Sound Pressure Level in 1/3 Octave Bands (db ref 2 x 10^{-4} dynes/cm^2)	Tolerance Band (db)	
80	132.5	+4	-4
100	136.0	+4	-4
125	138.0	+4	-4
160	140.0	+4	-4
200	142.0	+4	-4
250	142.5	+4	-4
315	143.0	+4	-4
400	142.5	+4	-4
500	141.5	+4	-4
630	140.0	+4	-4
800	138.0	+4	-4
1,000	136.0	+4	-4
1,250	135.0	+4	-4
1,600	133.0	+4	-4
2,000	132.0	+4	-4
2,500	130.0	+4	-5
3,150	128.5	+4	-5
4,000	127.0	+4	-5
5,000	125.5	+4	-5
6,300	124.0	+4	-5
8,000	122.5	+4	-6
10,000	120.0	+4	-6

2.1.2.3 Shock

The mechanical shock environment shall be the shock pulse shown in Figure 2-4, and shall be applicable to each of the three mutually perpendicular axes defined in Section 2.1.2.1.

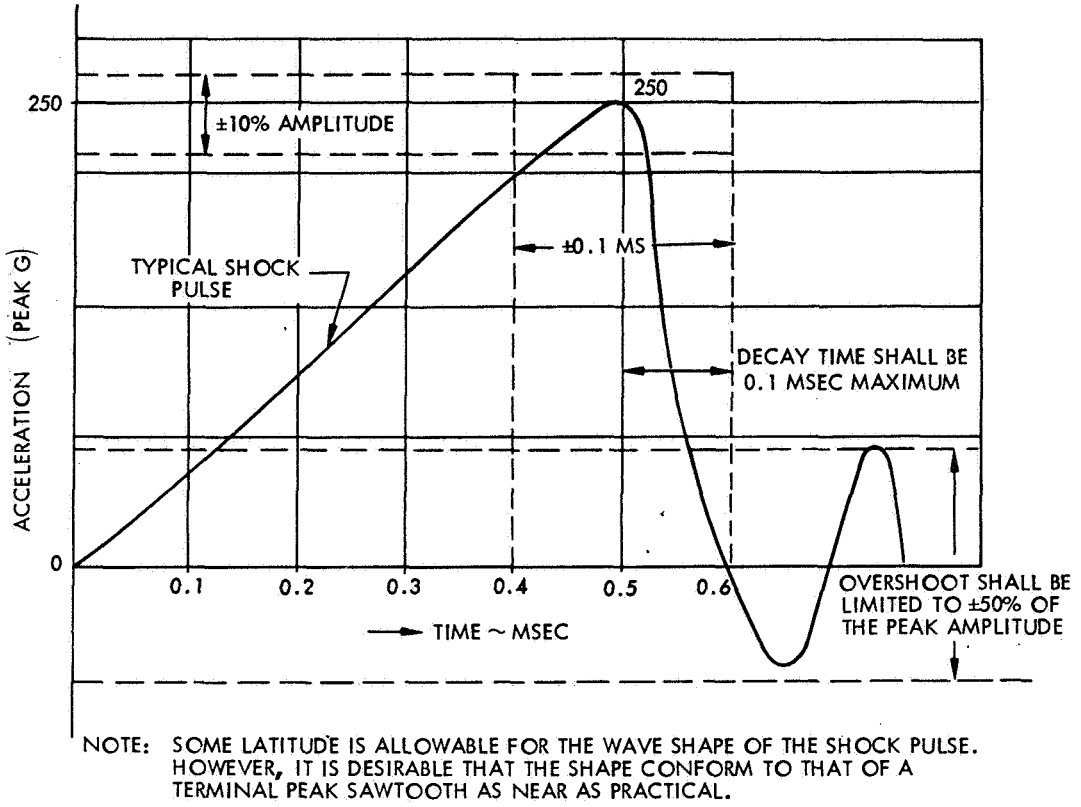

Figure 2-4. Shock Pulse

2.1.2.4 Static Acceleration

The static acceleration environment is 9 G's at the approximate center of mass of the subsolar array in the stowed configuration. This environment shall be considered equal for each of the three mutually perpendicular axes defined in Section 2.1.2.1.

2.1.2.5 Thermal-Vacuum Environment

The following represents the launch thermal-vacuum environment on the subsolar array in the stowed configuration.

2.1.2.5.1 Launch Pressure Profile

The subsolar array temperature shall be initially at +80 $\pm 10^{o}$F and atmospheric pressure. The pressure shall be continuously reduced and the rate of change of pressure shall obtain a maximum of 116 $\pm$8 torr/second beginning from a rate of less than 16 torr/second and returning to a rate of less than 16 torr/second in a period of less than 10 seconds and a minimum pressure level of 20 percent of the atmospheric pressure in less than 65 seconds.

2.1.3 AERODYNAMIC HEATING

The aerodynamic heating rate of the subsolar arrays external surface during boost in the stowed configuration shall be considered as $+30^{o}$C per minute for a period of 200 seconds. Initial temperature shall be taken at 27 $\pm$ 6^{o}C.

2.1.3.1 Space Flight Environment

The RA250 is to be designed to withstand the space environment encountered by interplanetary vehicles. The nominal mission length is 245 days and the system is to be capable of deployment and retraction at any time during the mission. The number of deployments and retractions is unspecified and is taken to be a small number.

2.1.3.1.1 Structural Characteristics

It is required that the resonant frequency of the RA250 in the deployed state will exceed 0.04 Hz. The structure is to be sufficiently rigid so that the array can be oriented by controlling the attitude of the spacecraft and its surface can be maintained within $\pm 10^{o}$ from the nominal plane surface of the array. This tolerance includes deflections due to thermal gradients. No acceleration environment has been defined for this program. In the feasibility study, a step acceleration of 2×10^{-5} rad/sec^{2} which could act for periods of 13 seconds to 5 minutes was specified. Analysis showed this to be a less severe requirement than the 0.04 Hz minimum natural frequency.

2.1.3.1.2 Thermal-Vacuum Environments

For design purposes in both the stowed and deployed configurations the steady state temperature range is -130^{o}C (-202^{o}F) to 140^{o}C (283^{o}F) with a rate of change up to 5^{o}C per minute.

Thermal shock temperature extremes shall be considered to be -130°C (-202°F) and 140°C (283°F). The temperature rates of change shall be the natural cooling rate of the RA250 in a passage through a planetary shadow and the natural heating rate of the RA250 in a normal solar flux of intensity corresponding to a steady state temperature of 140°C (283°F) on the solar cell blankets.

2.2 GENERAL DESCRIPTION OF RA250 SYSTEM AND SUPPORTING HARDWARE

The RA250 Rollup Solar Cell Subarray system provides the means to store (through launch), deploy, and support a 250 square foot panel of solar cells. The schematic arrangement of the system in the deployed configuration is shown in Figure 2-5. Solar cells are mounted on two flexible panels of Kapton [46.064 inches (3.85 feet) x 402.317 inches (33.526 feet)] Tension is utilized to maintain the desirable single-plane geometry and to establish the natural frequency of the system slightly above the required 0.04 Hz requirement. The tension loading is applied from within the storage drums and is resisted by the deployable structural elements. Six components are combined to form the power producing system: (1) the array blankets, (2) the single BI-STEM erection rod, (3) the storage drums, (4) the center support, (5) the leading edge member, and (6) the outboard support brackets. Specific performance of the system is 31.986 watts per pound (2500 watts/78.16 pounds). The noise fairing envelope is not a constraining factor for the RA250 design. The spacecraft mounting surface dimensions were a factor in the selection of the width of the RA250.

2.2.1 ARRAY BLANKETS

Each of the two solar cell array blankets accommodates six 102-volt circuits which feed to a common blanket mounted busbar. The power is transmitted along array-mounted busbars on the underneath side of the panel until it reaches the feedthrough interface on the drum skin. At the design operating point the current is 24.739 amps (power = 2523 watts) for the designated temperature of 55^{o}C. The array blankets are the major weight influence on the system contributing 42.04 pounds of the total 78.16 pounds. Interlayer cushioning buttons of foamed RTV 560 are bonded to the underside of the blankets to enable survival of the launch dynamics environments. Attachment to the drums is made by bonding. Attachment to the leading edge member is made by looping the Kapton substrate around it.

Fabrication of the array blanket proceeds along parallel paths with solar cell assemblies being brought to the module stage (19 parallel x 20 or 22 cells in series) and with the assembly of the substrate which includes the bus bars and the foamed rubber pads.

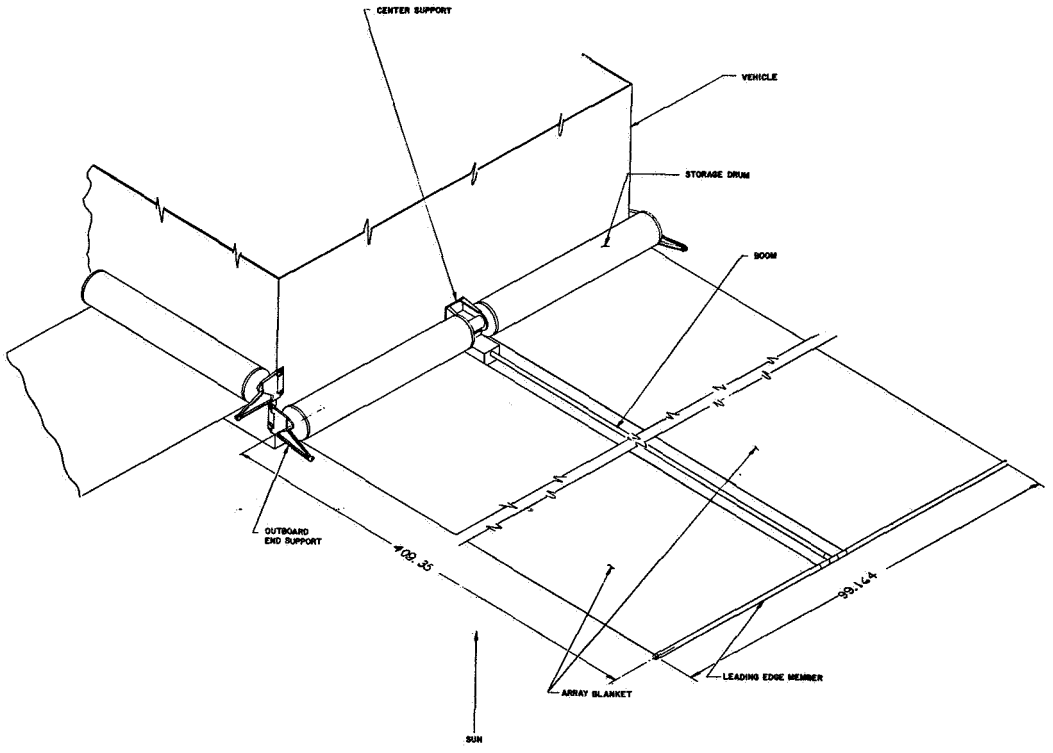

Figure 2-5. Subarray Assembly

Interconnection of the solar cells is by soldering of a formed silver mesh interconnection. The soldering process to be used is that of employing infrared as the heat source. Precise control of the ammount of solder is planned by pre-plating the interconnections, a method which shows great promise with regard to avoidance of localized solder accumulations. Modules will be electrically tested before bonding on the substrate.

The substrate starts as a sheet of Copper Clad Kapton (Schjelclad L7510) which is etched to remove all copper, except that of the busbar network. Busbar insulation and jumper connections are installed and the foamed RTV cushioning buttons are installed before the final assembly operation during which the modules are installed and interconnected.

2.2.2 BI-STEM ERECTION ROD

The backbone of the deployed configuration structure is the BI-STEM erection Rod (1.34 inch diameter, 0.007 gauge stainless steel) which provides the support strength and outboard and positioning control during the transition from stowed to deployed configurations. The rod strength is sufficient to overcome the tensioning forces transmitted through the array blanket throughout the 33.5 feet linear travel. Its strength is also sufficient to keep the out of plane geometry of the deployed configuration within the $\pm$10 degrees from its basic position normal to the spacecraft centerline.

The structural model for the BI-STEM is a pin-ended column for the space condition where the absence of a gravitational component results in a simple axial loading with the line of action passing through the ends. The tensioning force is four pounds, which assures that the natural frequency will exceed the 0.04 Hz specified.

In the "1 G" environment, the structural model closely fits the fixed-free column with its more severe buckling reaction. However the rod strength is such that unaided deployments can be performed while supporting the combined tension load and end rod weight load, but not the blanket loads. Counterweighting to compensate for the blanket load enables rod actuation of the array in the 1-G environment.

2.2.3 DRUM ASSEMBLY

The principal function which establishes the storage drum configuration is that of supporting the solar cell blankets during launch. An 8-inch-diameter configuration has been established based on prior vibration and acoustic testing. Stress studies established that "simple support" at each end of the drum resulted in the overall lightest configuration. The drum lengths are 47.1 inches, an inch wider than the blankets in order to accomodate provisions for free tracking during retraction. Additional features incorporated into the drum component are the blanket tensioning control through utilization of a negator spring and power transfer through the rotary joint between the array blankets and the spacecraft. The feedthrough consists of two harnesses and a slip ring assembly. Both power and telemetry signals are transmitted through the joint.

The inboard end assembly forms a major subassembly of the drum. This unit includes the stationary support shaft, on which are ground the bearing mounting diameters, the bearings, and the inboard end cap housing which rides on the bearing. In addition, the negator spring take up spool and back winding diameter are attached to the end cap and shaft, respectively, enabling inspection and test of this function at the subassembly stage. The slip ring and its feedthrough harnesses are also attached to the inboard end assembly allowing a complete electrical check of these components before their assembly into the drum.

The assembly sequence is to install the inboard assembly into the drum shell, and then to close the assembly with the installation of the outboard end cap. The array assembly is then mounted and connected to the drum with external operations.

2.2.4 CENTER SUPPORT STRUCTURE

The single point interface between the deployed subarray system and the spacecraft is provided by the center support structural component. The unit provides the mounting and electrical interfaces for the major system components, the drums and the BI-STEM erection rod. Construction is an aluminum box weldment with pads for the two drums on opposite sides and the pad for the BI-STEM at 90 degrees and in the same plane. The spacecraft mounting pad is on the side mutually at 90 degrees to the three component pads.

Pass-through access for the electrical harnesses which pass through the drum shafts is accomodated by holes in the weldment and the harness end connectors are mounted on the center support and become the spacecraft electrical interface.

Design sizing of the center support is controlled by the dynamic launch environments, and is currently being revised to ensure adequacy with regard to the present vibration environment.

2.2.5 LEADING EDGE

Support of the outboard ends of the solar cell blankets is provided by the 1.0-inch diameter leading edge member. The leading edge mounts through bearings on the outer end of the BI-STEM, thereby maintaining torsional freedom between the rod and blankets and allowing the tensioning to maintain the array blanket in the plane of the tangent to the drum. Construction of the leading edge is essentially that of a beryllium tube, the material choice being principally to achieve the stiffest member with the least weight penalty. Minimization of the droop deflection aids the uniformity of load distribution across the ends of the solar array blanket and ensures that the deployed dynamics characteristics are established.

2.2.6 OUTBOARD SUPPORT BRACKETS

The need for simple support of the drums and for caging of the outer ends of the blankets during launch is fulfilled by outboard support brackets which are engaged only during the stowed configuration. The brackets provide a direct structural tie to the spacecraft at the outboard ends of the drums and leading edge member. The attachment to the subarray components is by conical plug and socket joints to enable and unplug release as the initial function in the deployment sequence. A spring-loaded hinge joint actuated the release following a pyrotechnic actuation of a separation nut used to secure the stowed configuration lock-up.

2.3 ANALYSIS AND DESIGN

The results of analysis and design activities carried out during this period are discussed herein.

2.3.1 VIBRATION LEVELS AND STRUCTURAL LOADS

The major factor in the design of most of the structural elements of the system is the dynamic loads resulting from the specified vibration environment. The vibration environment for this project is significantly more severe than the environment specified for the Feasibility Study, and one of the earliest analytical tasks of this project was to assess the effects of the current environment on the design concepts previously developed. Both environments are shown in Figures 2-6 and 2-7. Figure 2-8 shows there has been a slight increase in the sine vibra tion level up to 225 Hz, and then a large increase in the level up to 27 G's from 550 Hz to 2000 Hz. These latter levels are a new consideration since the previous cutoff is the sine spectrum was 200 Hz. The change of most significance is in the random vibration test. As seen in Figure 2-7, there is a large "across-the board" increase in the power spectral den sity. In the expected resonant frequency range of the structure, the PSD level went from 0.1 to 1.0 G^2/Hz.

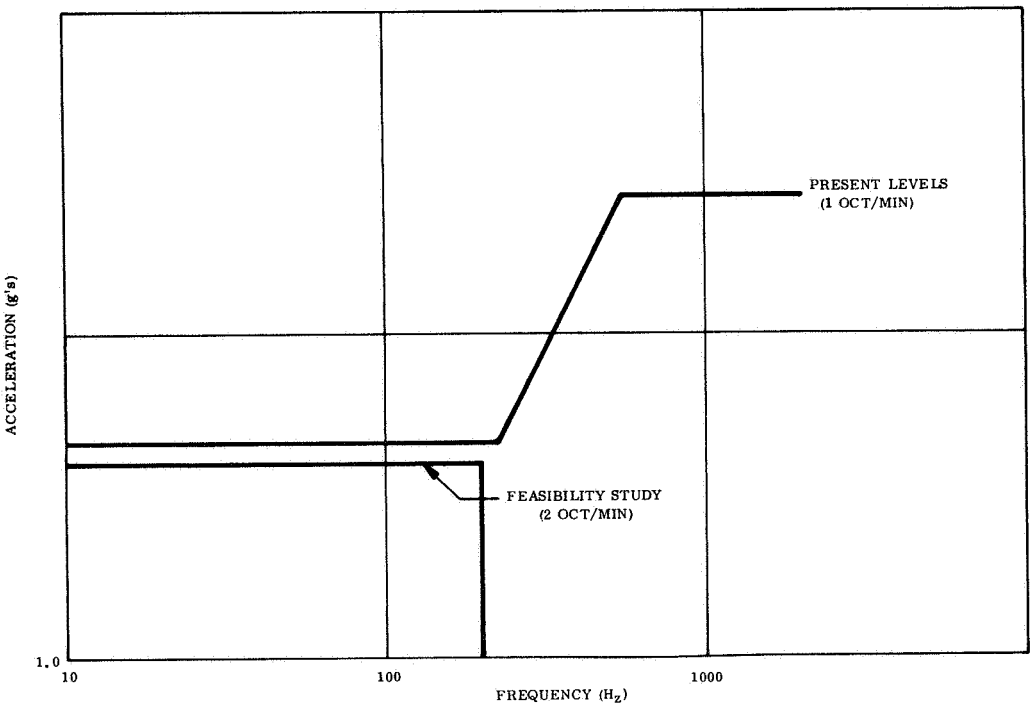

Figure 2-6. Sine Variation Levels of Rollup Subsolar Array

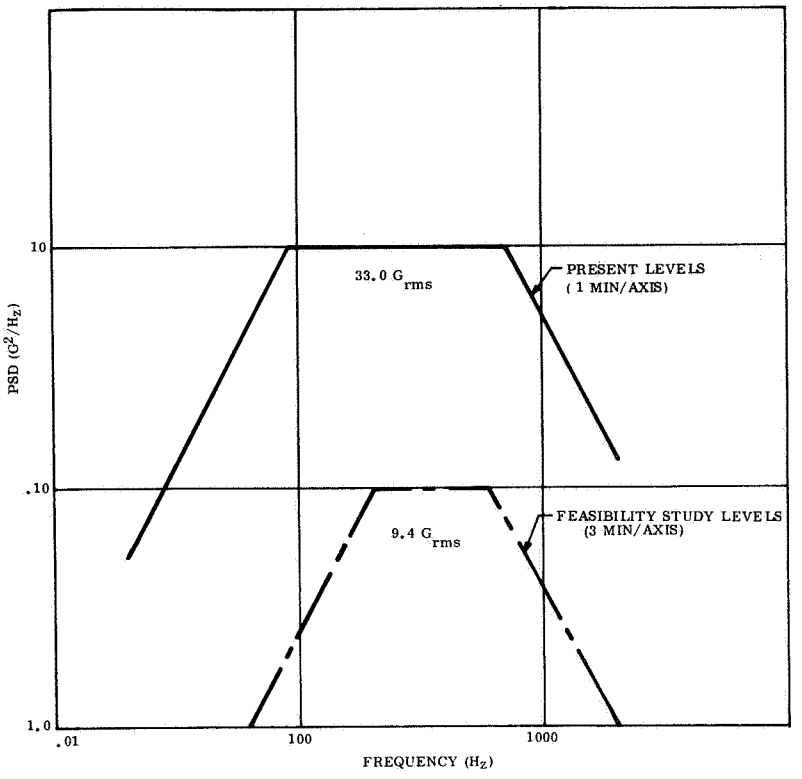

Figure 2-7. Random Vibration Levels for Rollup Subsolar Array

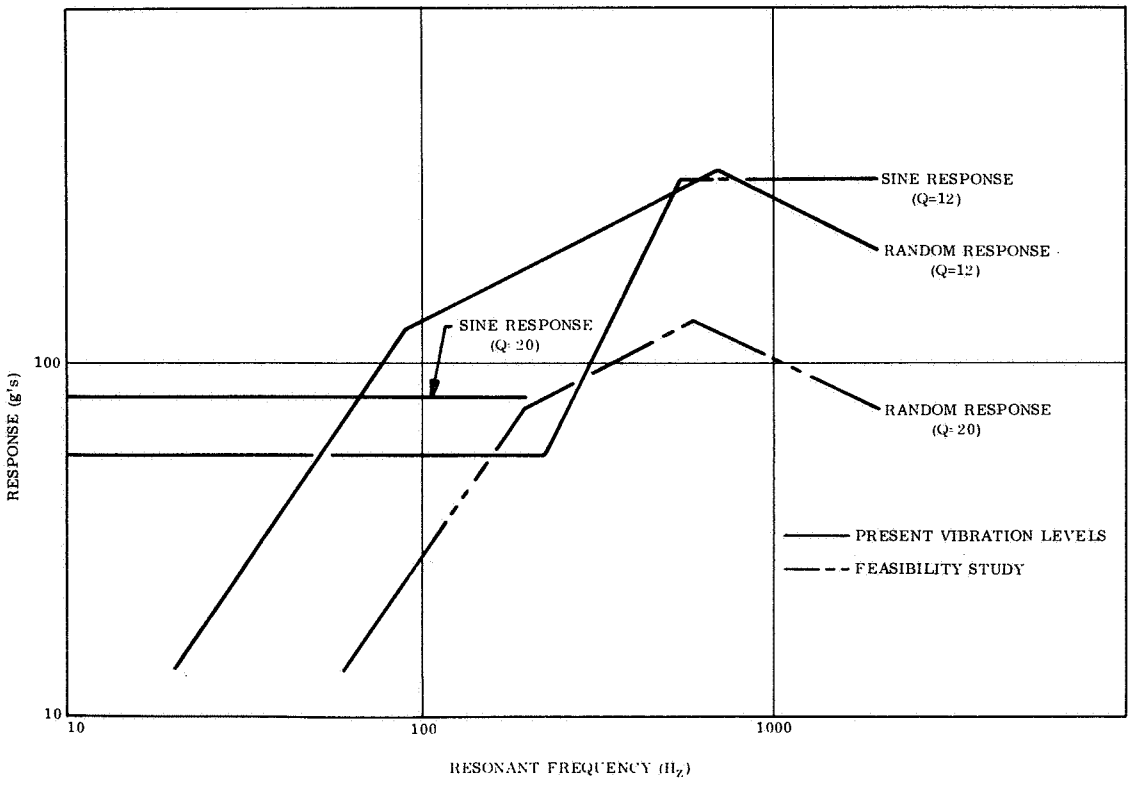

Figure 2-8. Structural Response as a Function of Resonant Frequency

To determine the effect of the increase in vibration levels in terms of structural loads, the curves in Figure 2-8 were developed. These curves represent both the sinusoidal and 3σ random response of a single degree of freedom system to the levels shown in Figures 2-6 and 2-7. As seen, the original design levels were higher in the low resonance range from 10-65 Hz; however, the new levels produce loads significantly higher for resonances of 65 Hz and above. As far as the rollup solar array structure is concerned, the loads will be increased by a factor of 2.5 in the structural resonant range of 200-225 Hz. It should also be noted in Figure 2-8 that the amplification factor (Q) has been reduced to 12, from 20. This lower value removes some of the conservatism present in the preliminary design analysis and is more representative of the amplification factors used on other spacecraft subjected to high vibration levels. It is this reduction in the amplification factor that resulted in an increase of only 2.5 in the structural loads. A straight ratio of the PSD levels would have resulted in a 320 percent increase in the loads.

The structural design philosophy of the Feasibility Study was to provide a natural frequency in the stowed configuration of 200 Hz or more. At 200 Hz, Figure 2-8 shows that the response to specified sinusoidal and random excitation levels would be approximately equal, and that above 200 Hz, there was to be no sinusoidal excitation. To implement this philosophy, stiffness in addition to light weight was desired. The present vibration environment leads to a different design philosophy. Over much of the frequency range where the first stowed natural frequency is expected to occur, the random response is the largest. The crossover point between the sinusoidal and random responses is near 50 Hz, a natural frequency lower than can likely be obtained with a system sufficiently strong to survive the environment. However, the dynamic loading decreases with natural frequency so that it is now desired to introduce flexibility into the stowed configuration. Materials and design selections from the Feasibility Study need to be examined with respect to the new requirements. A lightweight material with a lower modulus of elasticity than beryllium will result in a lighter weight system, because the dynamic loads will be reduced.

Component vibration levels were established for the solar panel actuator and the slip ring assembly and are shown in Figures 2-9, 2-10, 2-11, and 2-12. These vibration levels are based upon engineering judgments as to the effects of the mounting structure on the vibration environment input to the RA250 system.

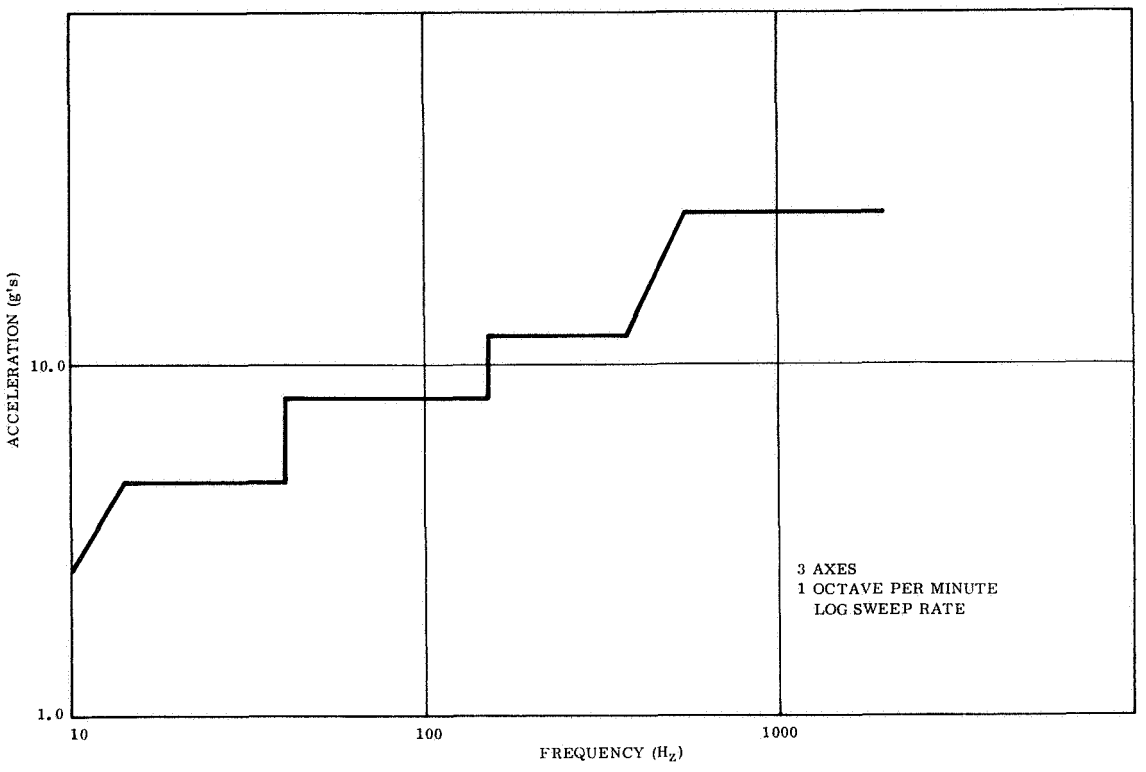

Figure 2-9. Sine Vibration Levels for Solar Panel Actuator

2.3.2 ANALYTICAL MODEL--STOWED CONFIGURATION

The initial dynamics analysis of the RA 250 system in the stowed configuration is used to determine the inertial loading conditions for use in stress analysis. The results will include the natural frequencies, the mode shapes, and the responses to sinusoidal and random excitation. The model also serves as the first iteration in the development of the final model for use in test planning and analysis of test results.

Because the array is symmetric about its centerline, a two-part model is used for the stowed configuration. One is for symmetric motions and the other for antisymmetric motions. These two parts are shown in Figure 2-13 along with the coordinate systems. The models

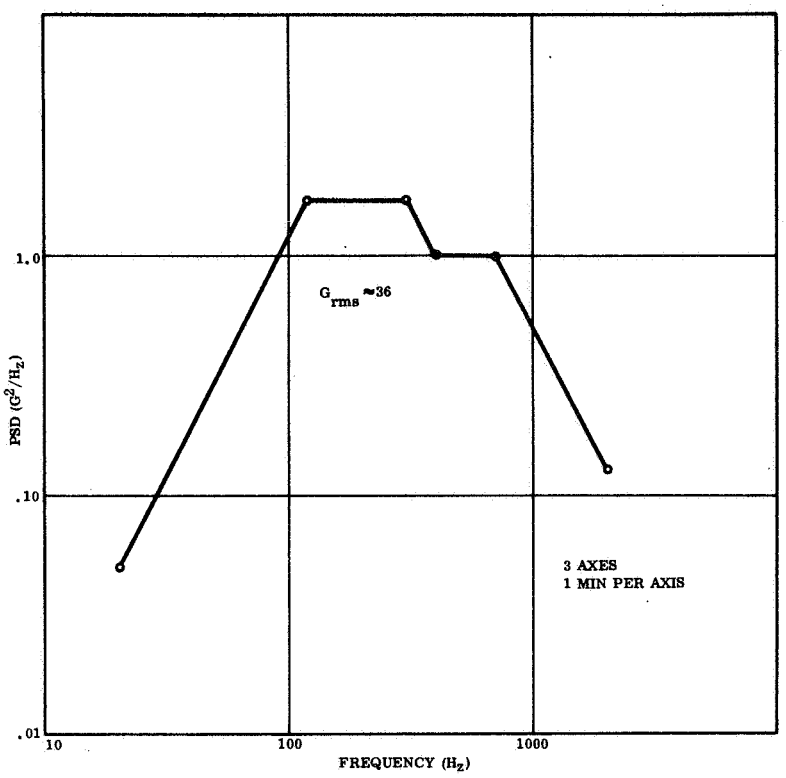

Figure 2-10. Random Vibration Levels for Solar Panel Actuator

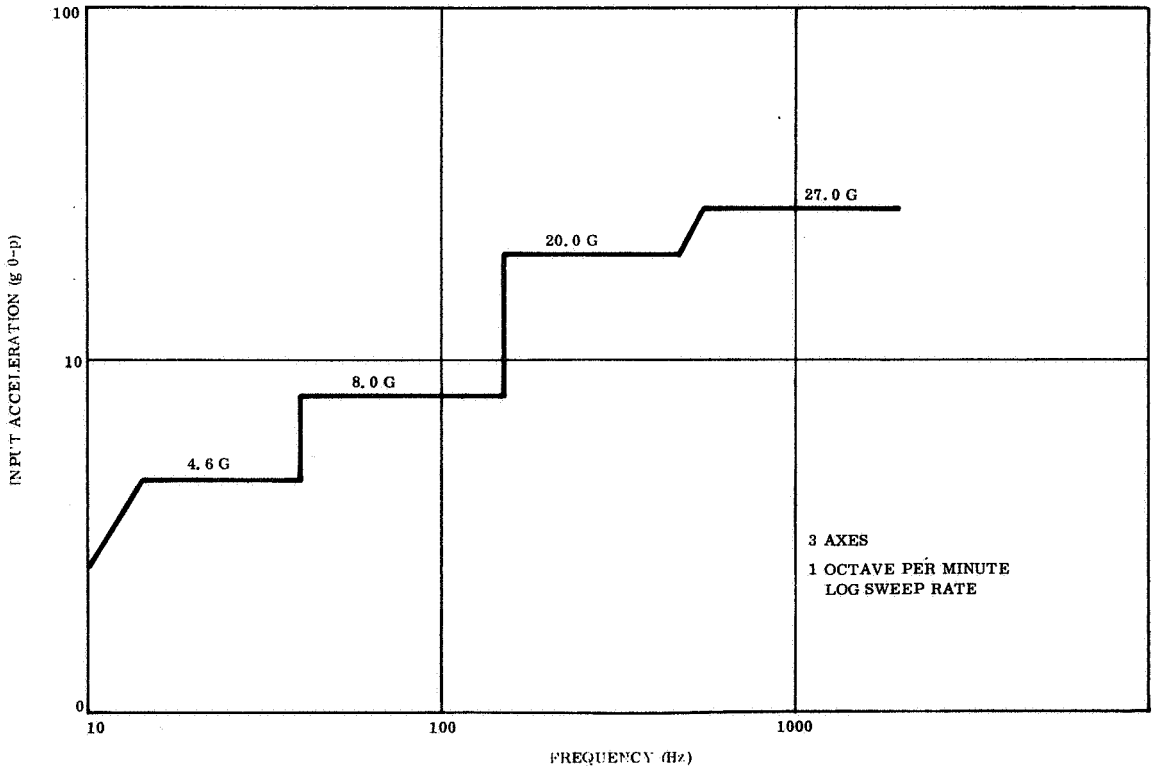

Figure 2-11. Sine Vibration Levels for Slip Ring

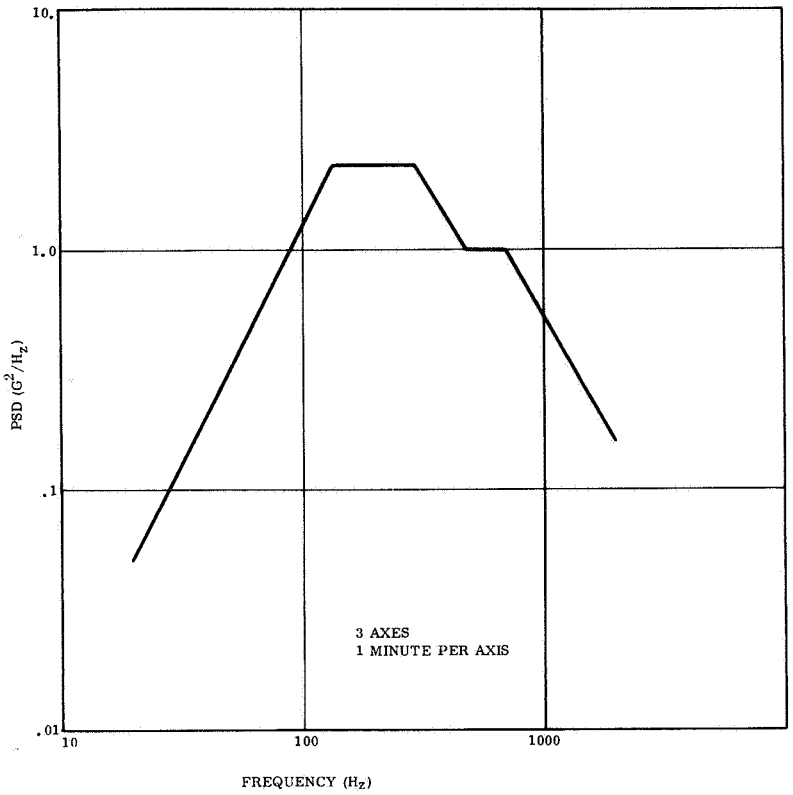

Figure 2-12. Random Vibration Levels for Slip Ring

developed in the Feasibility Study have been extended by allowing motion in two additional directions, X and Y. The inboard bearings are simulated by an equivalent spring between the hub and the drum with moments taken out through a couple formed by the two bearings.

The symmetric part consists of 33 degrees of freedom, while the antisymmetric part consists of 32 degrees of freedom. The degrees of freedom for the mass points are identified in Table 2-4.

Stiffness matrices for the model elements can be obtained with the stiffness matrix routine on the GE MASS structural analysis program. For example, the stiffness matrix for the outboard end supports has been developed. Figure 2-14 shows the configuration. The mathematical representation is made of a series of connected rectangular and triangular plates in the torque box section and two beams to form the support for the leading edge members.

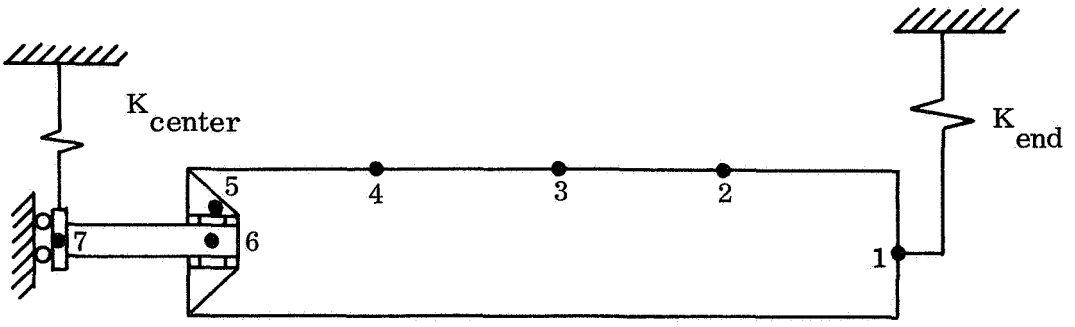

SYMMETRIC MODEL

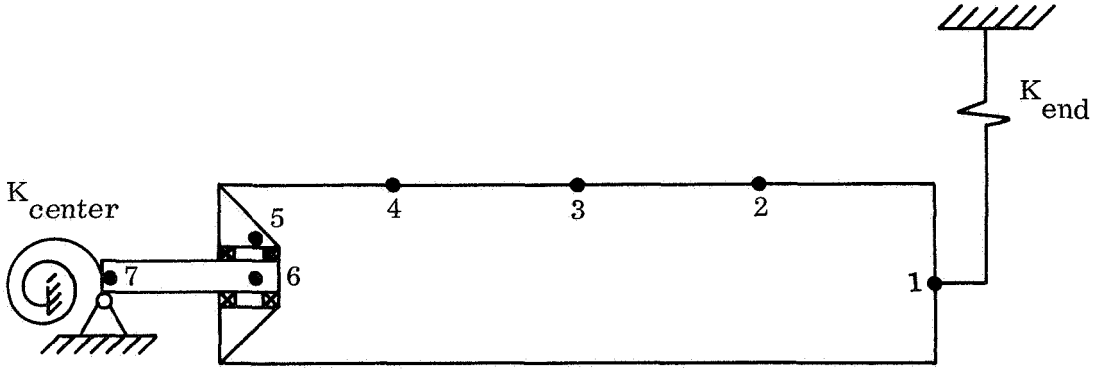

ANTISYMMETRIC MODEL

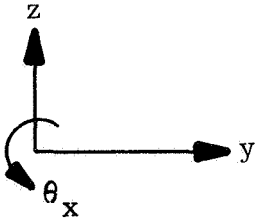

x - out of paper

Figure 2-13. Preliminary Mathematical Model

Table 2-4. Coordinate Identification

Mass Point	Coordinates Kept	
	Symmetric	Antisymmetric
1	$X, Y, Z, \theta_X, \theta_Z$	$X, Y, Z, \theta_X, \theta_Z$
2	↓	↓
3		
4		
5		
6	$X, Y, Z, \theta_X, \theta_Z$	$X, Y, Z, \theta_X, \theta_Z$
7	X, Y, Z	θ_X, θ_Z

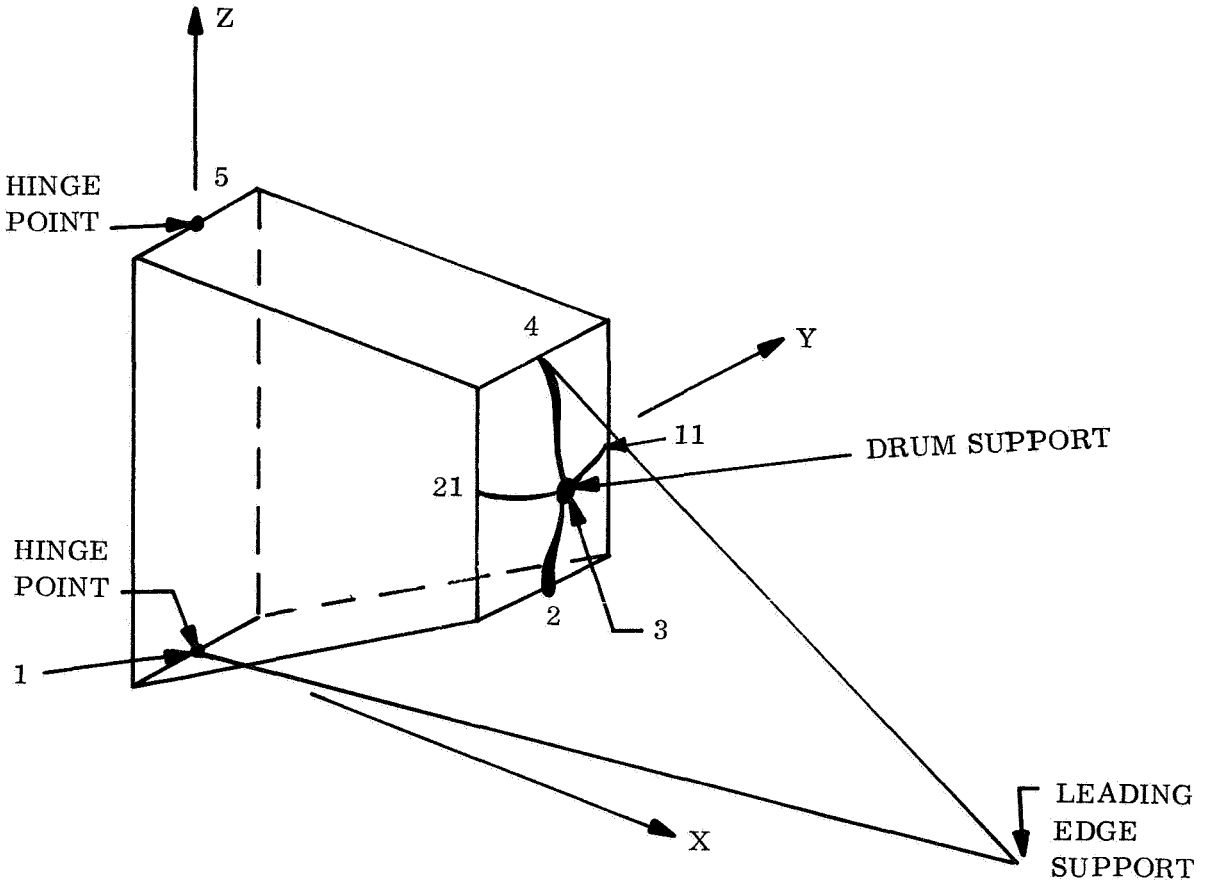

Figure 2-14. Outboard End Support

Node 3 was designed as the external joint for which the stiffness matrix was desired. This node is rigidly attached to the torque box by Members 3-2, 3-4, 3-11, and 3-21. The boundary condition at Node 5 provided restraint in the X and Y directions. The boundary condition at Node 1 reacted to loads in the X, Y, and Z directions and moments about the Z axis. The separation nut is located at Node 1. The resulting stiffness matrix, which is symmetric about the diagonal, is shown in Table 2-5.

Table 2-5. Stiffness Matrix for Node 3 of Outboard End Support

X	Y	θ_Z	θ_X	θ_Y	Z
0.48338E 06	0.23978E-01	0.25713E-01	0.45688E-01	0.29658E 05	-0.39436E 05
0.	0.12029E 05	-0.70775E 05	0.40268E 04	0.53434E-02	0.40153E-02
0.	0.	0.43201E 06	-0.30399E 05	0.27741E-01	0.62525E-02
0.	0.	0.	0.25701E 06	0.45762E-01	0.93672E-02
0.	0.	0.	0.	0.13026E 07	0.18186E 06
0.	0.	0.	0.	0.	0.17134E 06

2.3.3 ARRAY DESIGN AND PERFORMANCE

Electrical design of the solar array is complete, and mechanical design is in the final detail stage.

2.3.3.1 Electrical Performance

The solar cell subarray is composed of 55,176 cells combined into submodules (19 cells in parallel), modules (20 or 22 submodules in series), circuits (12 modules in series), and panels (6 circuits in parallel). The cells are 2 cm by 2 cm by 8 mils, N/P, 2 ohm-cm, of "bar contact" design. Figure 2-15 shows the composite current-voltage characteristic curve for AMO illumination at 55°C. The maximum power point of this curve is designated the design operation point and encompasses the following parameters.

Operating voltage (array)	102.0
Total array current (amps)	24.739
Individual circuit current (amps)	2.062
Array power (watts)	2523.0
Busbar voltage loss (percent)	2.0

For the prototype array which will be built during this program, only 10 percent of the array will be covered with working solar cells, the remainder being covered with glass wafers equivalent in mechanical dimensions and properties. The distribution of the working cells to the various zones of the array blanket, inboard, central, and outboard zones at edges or in the center will be by 15 isolated modules (19 cells in parallel by 20 cells in series). These will be connected into the distribution busbars and isolated by diodes to enable individual testing. The performance characteristic of the module and of the module in combination with the diode is shown in Figure 2-16.

2.3.3.2 Physical Configuration

The array consists of two panels, 46.064 inches wide by 402.317 inches long, with end connection pieces extending beyond the cells at both ends. Each panel carries six circuits each of 242 cells in series by 19 cells in parallel. Each circuit is composed of twelve series-connected modules (eleven 20 series by 19 parallel and one 22 series by 19 parallel). Connection of the circuits into the common busbar and interconnections between modules of each circuit are achieved through use of Schjelclad (L7510) Kapton-copper laminate. Interconnections between series rows of cells are 0.002-inch thick silver mesh.

A revision to the substrate construction approach of the Feasibility Study is being undertaken to improve the quality of the unit with regard to flatness and wrinkles. In place of the previously bonded busbar strips, the presently planned substrate will start as a Kapton-copper laminate and will achieve the busbar layout by photoetching away the spaces between the busbar runs. With this configuration, connections from the cell side of the panel to the busbar system will be around the edges rather than through holes in the substrate.

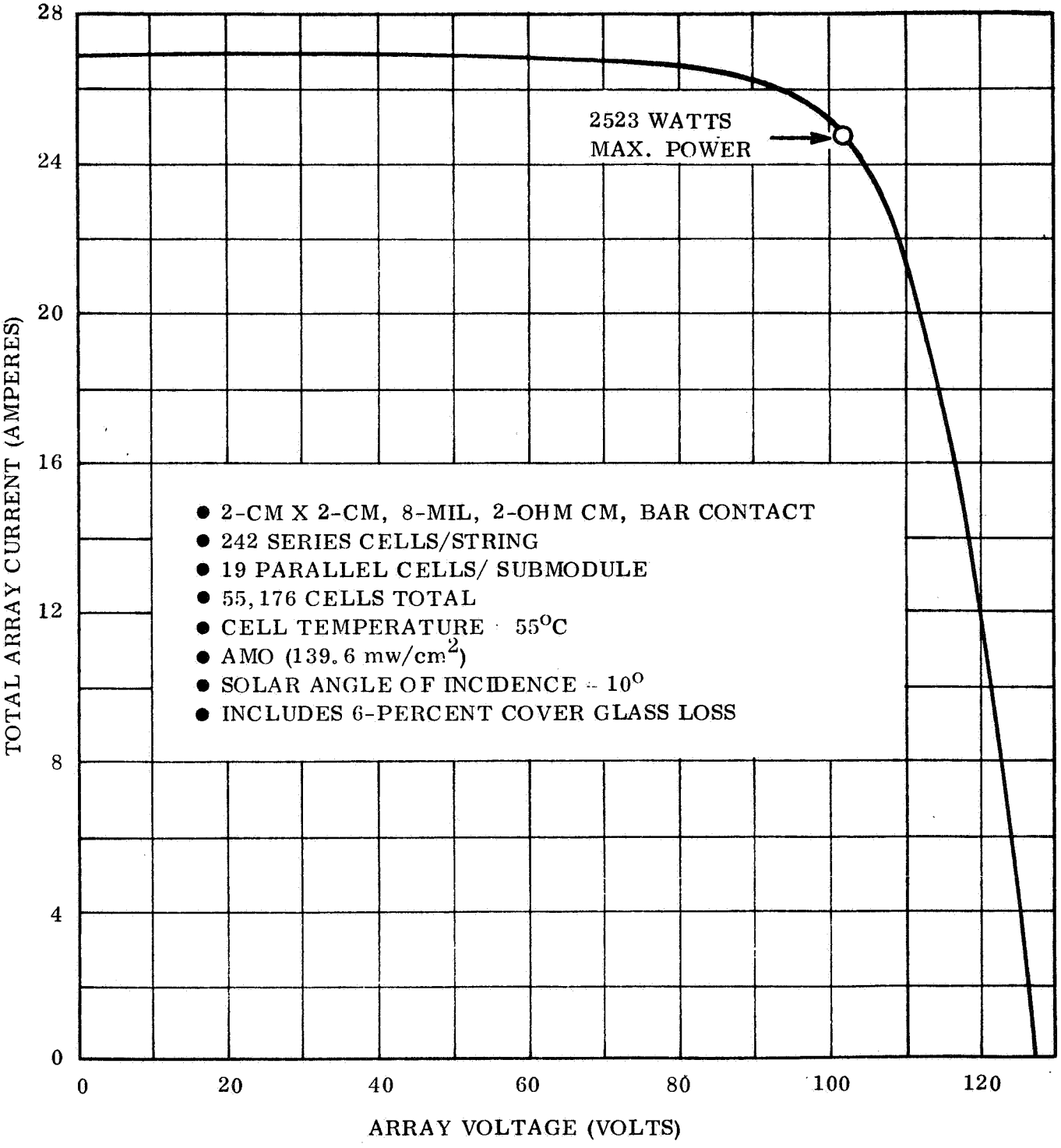

Figure 2 15. Array I-V Curve, 2-Ohm Cm, 8 Mil

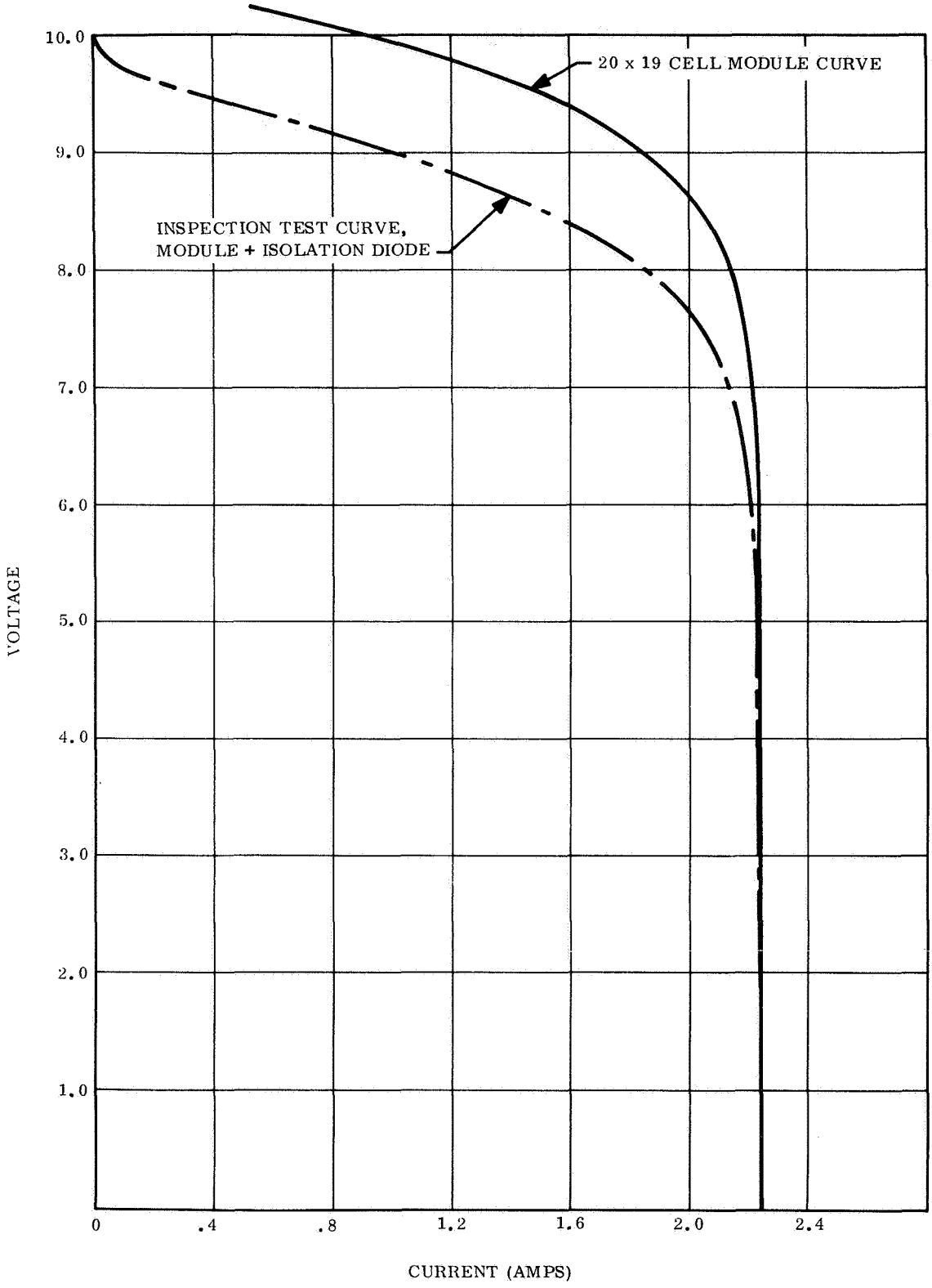

Figure 2-16. I-V Characteristic 20 Cell Series by 19-Cell Parallel Module, 55°C, AMO

The busbar system is essentially a river-tributary system, with each circuit feeding into the common bus, which in turn connects to the power feed through at the drum. Individual circuit diode isolation is not presently planned. Additional busbar runs have been added to the substrate to enable installation of high- and low-range thermistors on the panel. These also connect to the feedthrough section of the drum and the signal slip rings.

Detail drawings for the substrate-busbar unit, modules, interconnections, cells, and cover slides have been made.

2.3.3.3 Hot Spot Analysis

Initial studies of the implications of the "hot spot" solar array phenomenon to the planned array configuration have been completed. This phenonemon is the increase in temperature that occurs when portions of a solar array series string are forced into a reverse voltage condition because of electrical mismatch. The electrical mismatch can be caused by individual cell failures or by shadows which cover only a small fraction of the series string. The localized heating for one, two, and three cells, faulted in a single submodule, are shown in Figure 2-17 plotted against the temperature of the heating cell. A worst-case thermal model, that of heat rejection only by radiation and only from the heating cell, is also plotted. The intersection points between the hot cell heat generation curves and the thermal model establish the worst-case potential temperature. The solder melt range is also shown for reference.

As shown by the worst-case potential temperatures, the rollup subarray design (242 series by 19 parallel circuits) is insensitive to single-cell faults. For double-cell faults in a single submodule, the worst-case potential temperature approaches the solder melt range. However, recent tests on a conventional array (honeycomb substrate) show that there is a considerable heat flow to adjacent rows of cells which then share the heat rejection load with the heating cells. It is expected that the interconnection alone will pass a substantial fraction of the generated heat, so the two-cell fault will be shown clearly safe.

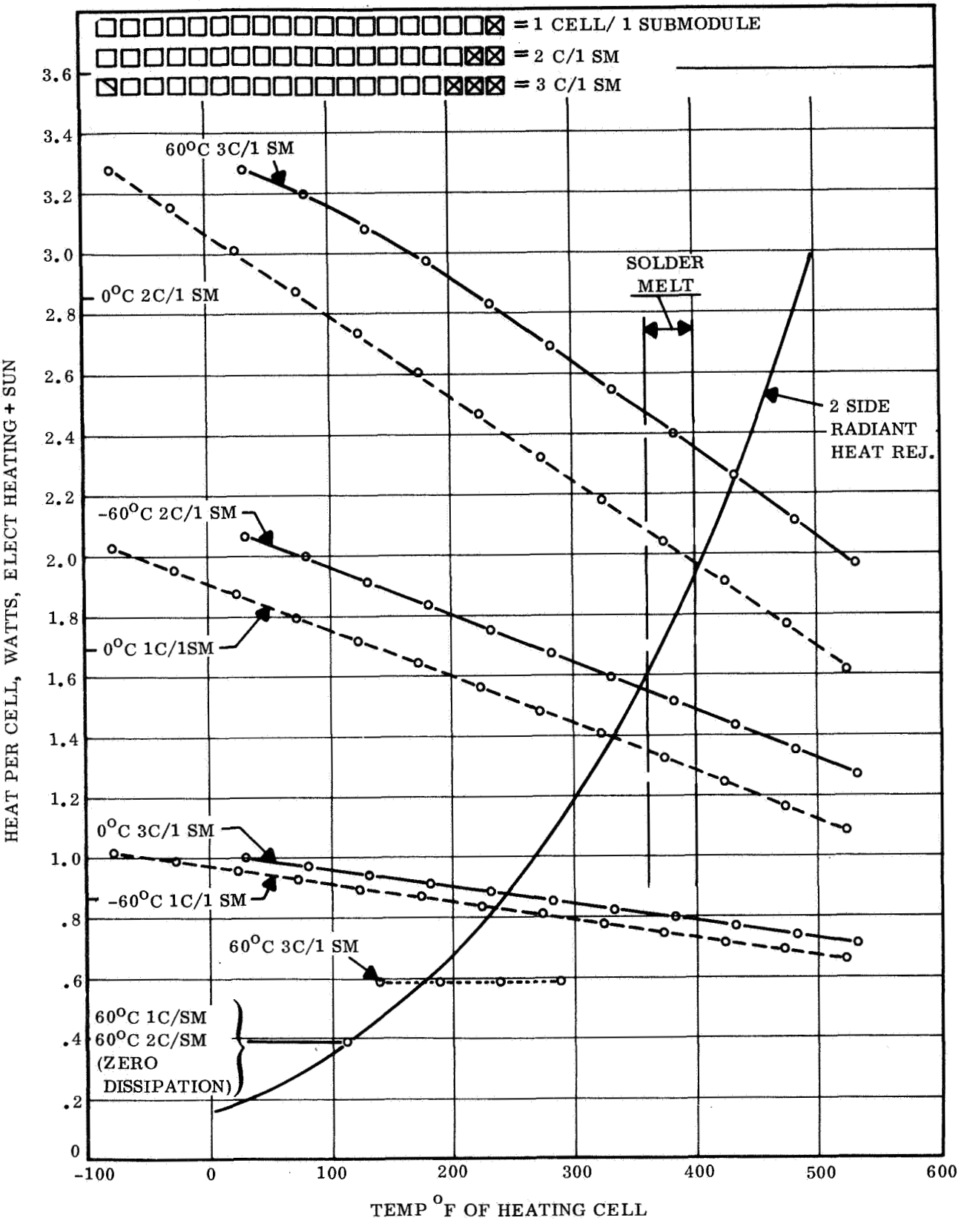

Figure 2-17. 30 Watt/Pound 19 Parallel by 242 Series "Hot Spot Study"

The honeycomb panel test also showed there was a tendency for the shunt resistance of the heating cells to fall off with increasing temperature. This reduces the negative voltages because more current is passed. The analytical curves which are based on a constant shunt resistance are pessimistic.

In view of the analysis and the recent test experience, it is concluded that the "hot spot" is not a potential failure source in this design, and therefore, use of bypass diodes to protect against it is not necessary.

2.3.4 COMPONENT DESIGN AND PERFORMANCE

2.3.4.1 Introduction

This section includes summaries of the following component design studies:

1. Bearing selection
2. Bearing lubrication
3. Spring motor analysis
4. Thermal cycling tests of solar cell blanket segments
5. Solar panel actuator
6. Slip ring assembly

2.3.4.2 Bearing Selections

The bearing for the main shaft/drum, as a first choice, is the split ball bearing 3TAO-49-62, selected for its light weight, capability of withstanding the dynamic loads, and compatability with the proposed design.

The bearings for the leading edge member and the spring motor takeup drum is the Barden SR6, selected for its size, which simplifies the motor drum design; for its adaptability to both leading edge member and motor drum; and for its availability in stock.

A study was completed to determine the optimum dimensions for a given shaft, housing, and bearing configuration which would yield the lowest weight for the present vibration loads.

The configuration for the inboard end cap and shaft presented in the Feasibility Study, Reference 3, was used, except that a standard non-preloaded bearing installation was analyzed. See Figure 2-18.

Volume equations were developed as a function of shaft length and bore. It was assumed that all wall thicknesses were on an average of 0.1 inch.

The resulting curves on Figure 2-19 show the effect on shaft and housing volume with changing shaft bore and length.

Table 2-6 summarizes the relative change in weight of shaft, housing, and bearings for each drum assembly. The weights calculated are not exact, but approximate the general design. They are used to exhibit the relative effect configuration dimension changes on weight to determine if further optimization should be pursued.

Table 2-6 (in conjunction with Figure 2-18) shows that the bearings are the main weight contributor, and that the variation in shaft and housing dimensions (within the constraints necessary to meet other requirements, such as array curvature and moving part clearances) has little effect on overall weight. Furthermore, since bearing weight is fixed, and housing and shaft can be detailed further for weight reduction, the bearing with the least weight, which will carry a 3,900-lb thrust load, is selected.

The split ball bearing SBB3TAO49-62 is the first choice for the main shaft and inboard end cap for the following reasons:

1. Weight is minimal for the imposed loads (0.26 lb for T_o =3,900 lb, C_o = 2,430 lb).
2. Large bore diameter (3.06-inch) provides greater access for wire routing through shaft.
3. Allows use of most of proposed design concept which has been analyzed.

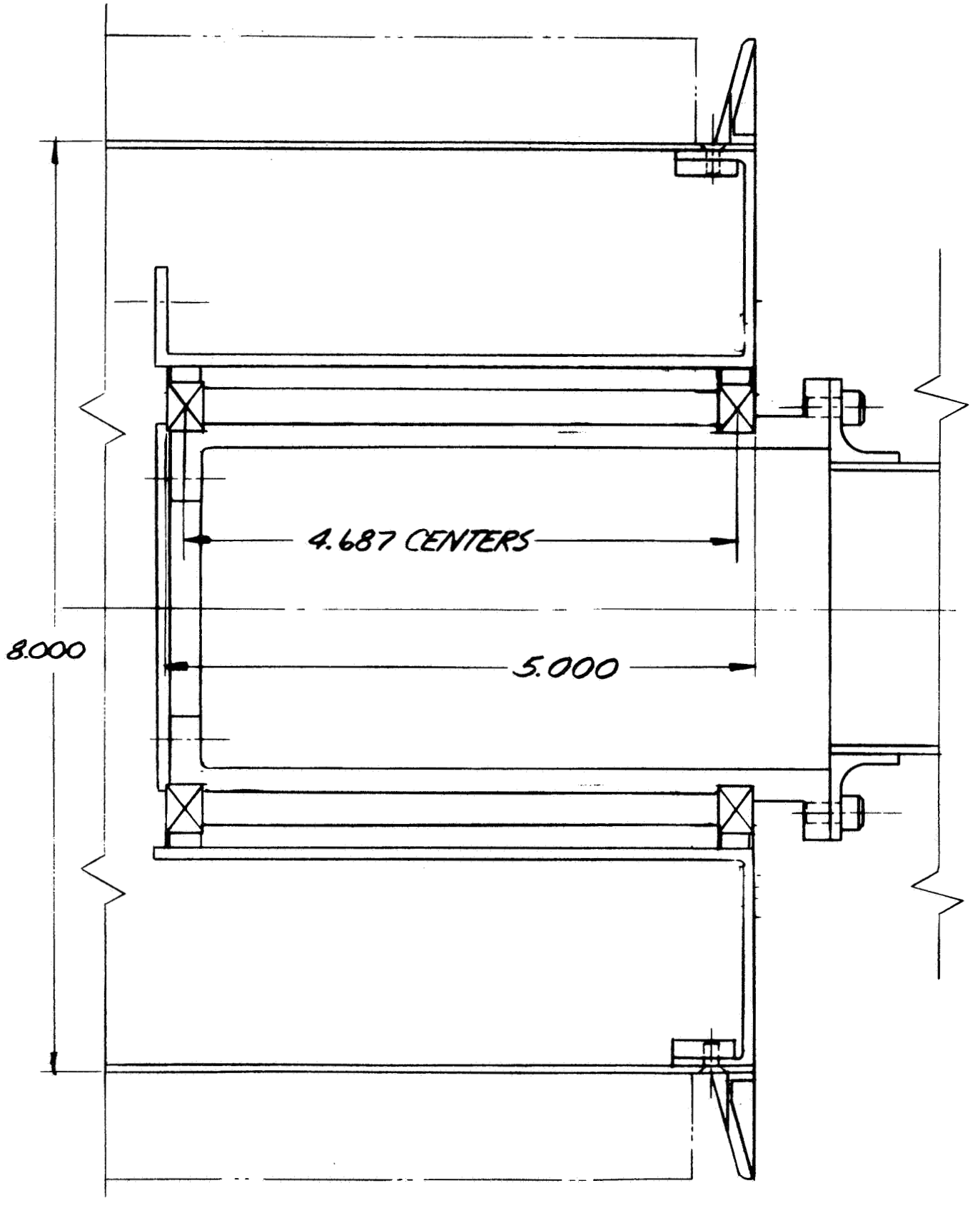

Figure 2-18. Bearing Arrangement for Inboard End Cap and Shaft

Table 2-6. Weight Change Summary

Bearing Data From Manufacturer					Shaft Length (in.)	Bearing ℄ Distance (in.)	Radial Load (Limit) Compare With Co (lb)	Shaft Bore ID (Wall Thickness = 0.125) (lb)	Material Vol. (Figure 2-18) ($in.^3$)	Material Wt. (Mg Alloy @ 0.065 $lb/in.^3$) (lb)	Total Relative Weight (lb)
Typical Bearing	C_o (lb)	Width (in.)	ID (in.)	Bearing Weight							
HDB-108	4,850	0.71	1.57	0.43	3.1	2.4	4,750	1.32	12.4	0.81	1.67
HDB-110	4,700	0.62	1.97	0.59	3.25	2.6	4,330	1.72	13.5	0.88	2.06
HDB-109	4,160	0.63	1.77	0.54	3.50	2.9	3,980	1.22	12.9	0.84	1.92
HDB-012	4,320	0.51	2.36	0.78	3.50	3.0	3,820	2.11	14.9	0.97	2.53
HAB-011	3,940	0.51	2.16	0.57	3.50	3.0	3,820	1.92	14.4	0.94	2.08
TAO49-62	2,500	0.31	3.06	0.26	5.0	4.7	2,430	2.71	18.8	1.22	1.74

NOTES

1. Radial load = $\frac{11,400 \text{ lb}}{\text{Distance between bearing centerline}}$
2. Bearing must be capable of taking 3,900 lb thrust load
3. Total relative weight = material weight + 2 x bearing weight

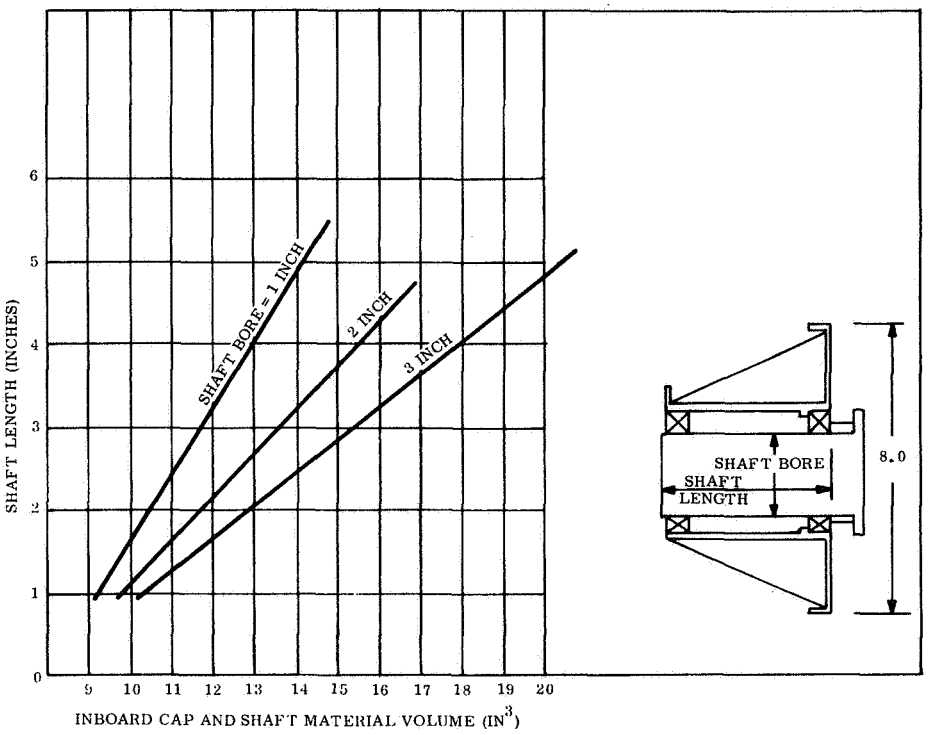

Figure 2-19. Parametric Study of Proposed Configuration Parameter Variation Effect on Relative Weight of Inboard Cap and Shaft

The bearings to be used in the spring motor takeup drum and the leading edge members are selected based on:

1. Use of the same bearing
2. Standard sizing (and tolerance) availability
3. Static load (large field) capability greater than 50 lb (radial and thrust)
4. Simplicity of installation and housing design.

Bearing vendor catalogs indicate several small instrument bearings which meet the above criteria. Since all are less than 0.05 lb, weight is not an important selection criteria. A bearing which meets the above requirements and is available in stock is the Barden SR6SSTB.

This size bearing is ideal for the motor drum in that its OD of 0.8750-inch and the required 1.31-inch OD of the drum allows for a minimal wall thickness of the housing where:

Bearing OD = 0.8750
Insert OD = 0.9610
Drum OD = 1.310

Wall thickness $\simeq$ 0.150 inch

Table 2-7. Bearing Summary

	Main Shaft	Leading Edge Member and Spring Motor Drum
Identification	SBB-3TA049-62	Barden SR6
Type	Angular	Deep groove
Mounting	Non-preload	Non-preload
C_o rated	2,500 lb	167 lb
T_o rated	4,680 lb	259 lb
C_o applied	2,430 lb (Bearing Ψ = 4.69 in.)	< 50 lb
T_o applied	2,900 lb	< 50 lb
Weight (Approx.)	0.26 lb	0.03 lb
Material	A1S1440C Stainless Steel	A1S1440C Stainless Steel
Retainer	Molydisulfide (Duroid 5813)	Molydisulfide (Bartemp)
Radial play	Later	0.0002 -0.0004
Torque friction	0.1 to 0.15 in.-lb (From vendor) For preloaded pair	0.048 in.-lb (Calculated from catalog)
Tolerances		
OD	+0.0000, -0.0004	ABEC 5
ID	+0.0001, -0.0003	ABEC 5
Speed	< 6 rpm	N/A-Leading edge < 10 rpm-motor

2.3.4.3 Bearing Lubrication

A review of the lubrication requirements of the ball bearings to be used on the RA250 has led to the conclusion that adequate reliable lubrication can be provided through the use of ball separators of RT/Duroid 5813, a reinforced-PTFE-MoS_2 compact material which provides a transfer-lubricant film on the ball and race surfaces. Test data and flight experience are discussed to support the selection of this material. The principal advantages of Duroid over the originally proposed lubricant (Lubeco 905) are: (1) ease of preparation of the bearings, (2) enhanced reliability of bearing parts through minimized handling, and (3) reduced procurement time and difficulty.

A long-life bearing evaluation program has been conducted at GE-MSD in which the operating characteristics of ball bearings with a number of dry lubricants were determined in hard vacuum ($\leq 10^{-9}$ Torr.) In this test program, both bonded or plated lubricants and transfer film lubricants were evaluated. Lubeco 905 (Lubeco, Incorporated, Compton, California), the lubricant originally proposed, showed good performance, as did certain other bonded or plated films. Among the transfer lubricants, RT/Duroid 5813 (Rogers Corporation, Rogers, Connecticut) demonstrated superior performance. The Duroid material (which is also marketed by Barden Corporation under the name "BARTEMP") is a glass-reinforced polytetrafluorethylene (PTFE) impregnated with molydenum disulfide (MoS_2). The material, which is fabricated into ball separators, provides a continuously rubbed film of PTFE and MoS_2 to the moving ball surfaces, which in turn transfer lubricant to the raceways of the bearing. While this is an effective lubricating mechanism in air, the GE tests have demonstrated even lower operating friction in vacuum.

In the GE tests, the Duroid lubricants were the only transfer lubricants, of three materials tested, which did not evidence significant increases in starting torque as a function of dwell duration under static load in vacuum.

Other investigators, including Clauss[4,5], Vest and Ward[6], and Scibbe[7], have also shown good test results in hard vacuum with ball retainers of this type of material. In the more recent tests by Clauss[5], bearings were subjected to severe vibration in both air and vacuum at +200°F, -200°F, as well as at room temperature. The Duroid material performed successfully throughout each 1000-hour test. These results serve to demonstrate the stability and adhesion of the PTFE-MoS_2 transfer film under extremes of temperature and severe vibration.

Vest and Ward demonstrated the adequacy of the transfer lubrication provided by glass-filled PTFE-MoS_2 retainers at low rotational speeds (< 1 rpm) and under limited oscillatory motion. These tests were successfully conducted in vacuum for periods in excess of 8000 hours.

Scibbe demonstrated the adhesion of PTFE transfer films under conditions of severe thermal shock and also proved the ability of transfer films to provide boundary lubrication in cryogenic reducing environments which would effectively remove lubricating oxides rapidly.

Actual flight applications using Duroid ball separators have included use on Surveyor, Nimbus, Apollo, and in many flight experiments. Portions of the OSO "H" Spectroheliograph are also employing this lubrication technique.

In order to ensure adequate control of the uniformity, constituency, and thickness of bonded or plated dry-lubricant films, it is necessary at this time to completely disassemble the bearing (which is an extremely critical process, involving some risk of loss) and coat the races and retainer parts with the dry lubricant, then subject every lubricated part to a thorough microscopic visual inspection[8]. The bearing must then be carefully reassembled without damaging the lubrication film, run-in, cleaned, and torque-tested to demonstrate proper assembly and lubrication. All these tasks are essentially the bearing user's responsibility, since bearing vendors in general do not perform this sort of processing.

In contrast, bearings employing transfer film lubrication can be purchased as relatively standard items from several bearing vendors, who maintain complete control over the bearing throughout assembly and test. Inch-series precision instrument bearings are available in several sizes from Barden Corporation, and Split Ball Bearing Division of MPB, Incorporated, can fabricate many of their large-diameter, thin cross-section bearings with toroidal Duroid separators around every secondball. The latter type of bearing-retainer arrangement is shown in the large bearing in Figure 2-20 while Figure 2-21 shows a disassembled miniature bearing with Duroid retainer. (The bearing shown in Figure 2-21 is actually the same size as the small bearings shown in Figure 2-20.

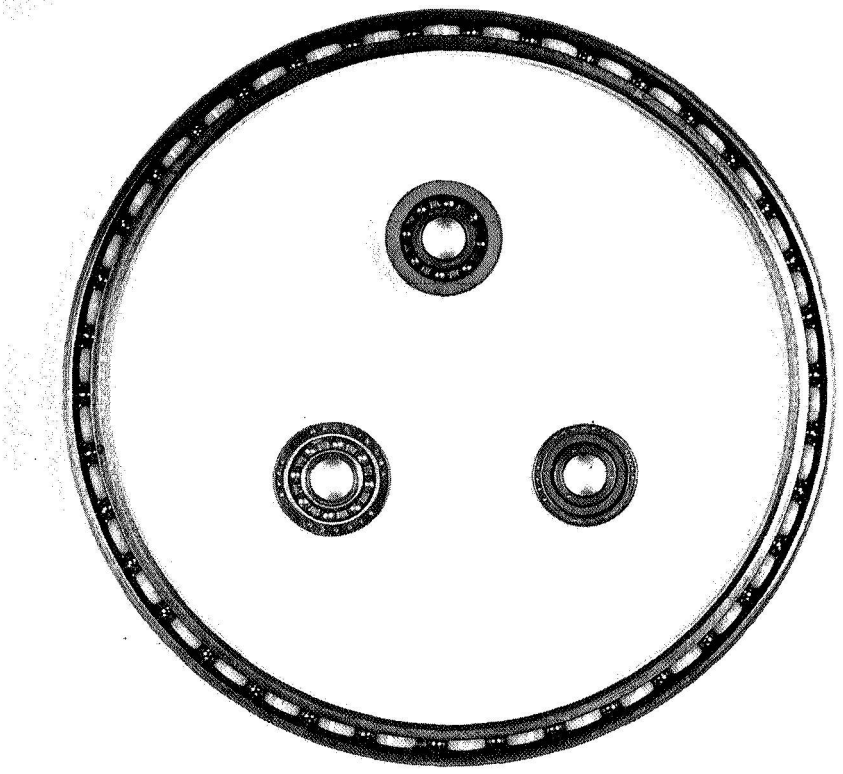

Figure 2-20. Self-Lubricating Toroidal Ball Separators Used on Alternate Balls in Large Bearing

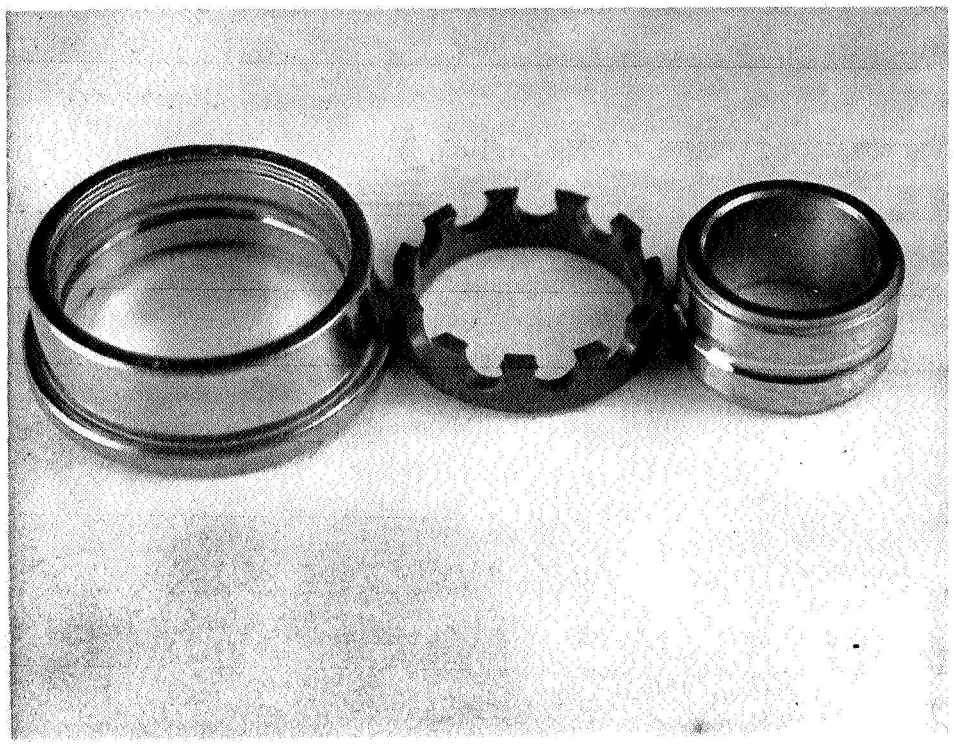

Figure 2-21. Self-Lubricating One-Piece Ball Separator/Retainer Used in Precision Instrument Bearing

2.3.4.4 Spring Motor Analysis Summary

Total Estimated Torque Requirement

2-lb tension load in array	=	8.00 in.-lb maximum
Main bearing friction	=	0.15 in.-lb
Slip ring friction	=	0.70 in.-lb
Spring motor bearing friction	=	0.096 in.-lb
		8.946 in.-lb

Since the 2-lb tension load for the array is maximum and can operate at 7 in.-lb, a 9 in.-lb spring is selected, allowing a margin for any spring hysteresis which is to be determined.

Main bearing friction was obtained from the SBB Engineering Group ans is derived from test data.

Slip ring friction is in accordance with the maximum allowable by the component specification.

Spring motor bearing friction is calculated from vendor catalog data, but does not include temperature effects or effect of solid lubricant.

Motor Sizing (based on Hunter spring catalog data)

Torque	9 in.-lb
Output drum OD	2.18 inches
Takeup drum OD	1.31 inches
Width of spring	1.25 inches
*Length of spring	131.8 inches + margin
Weight (approx.)	0.50 lb
*Distance between drum ℄s	2.75 inches
Spring thickness	0.010

*To be verified by vendor.

2.3.4.5 Thermal Cycling Tests of Solar Cell Blanket Segments

The thermal environmental limits for the RA250 program are -130°C (-202°F) and +140°C (283°F) for both steady state and thermal shock conditions. Several array segments have been subjected to thermal cycling tests with the goal being the development of interconnections which could withstand the repeated cycling of temperatures in the -200°F to -250°F range.

Three modules sized to fit the Engineering Laboratory thermal cycling chamber were constructed and tested. The first used solder plated photoetched Beryllium Copper interconnections, (Figure 2-22). It was typical of array construction except for the omission of cover glass. Half of the cells developed cracks during thermal cycling. The omission of glass was suspected to be associated with the failures. As a sensitivity of the array to the structural contribution of the cover glass had not previously been suspected, a second module using silver mesh interconnections, (Figure 2-23), was constructed without glass and subjected to the same test. The need for glass was again vividly demonstrated by the cracking of six cells.

The task was refocused on the original goals by the testing of a third module constructed with 8 mil cells, 6 mil cover glass, and silver mesh interconnections. This module was subjected to tests of at least 100 cycles over each of the following five temperature ranges:

1. +200°F to -200°F
2. +200°F to -210°F
3. +200°F to -220°F
4. +200°F to -230°F
5. +200°F to -240°F

No definite degradation occurred until the -240°F test, during which a cell crack across the negative interconnection developed.

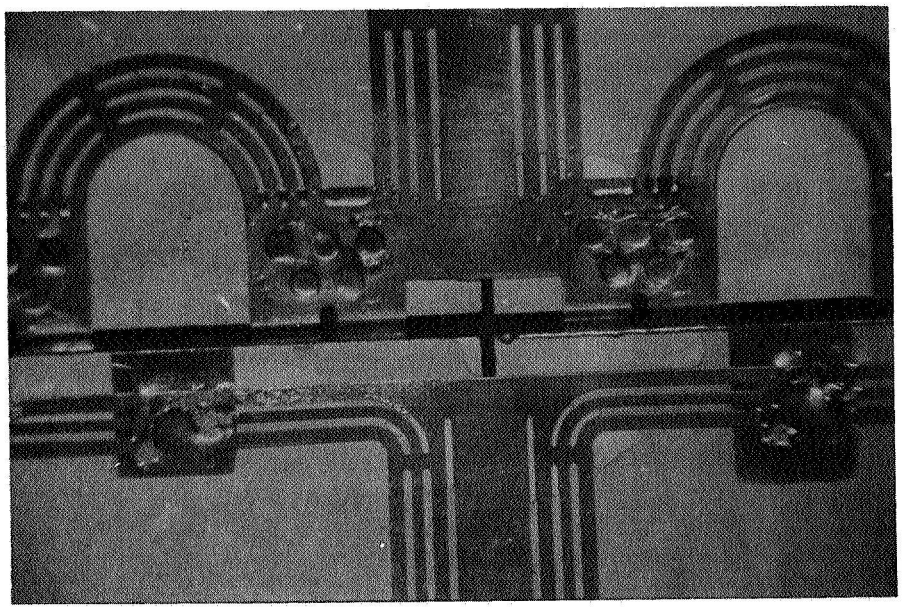

Figure 2-22. Closeup of Photoetched Solder Plates Interconnection (Back Side of Cell View)

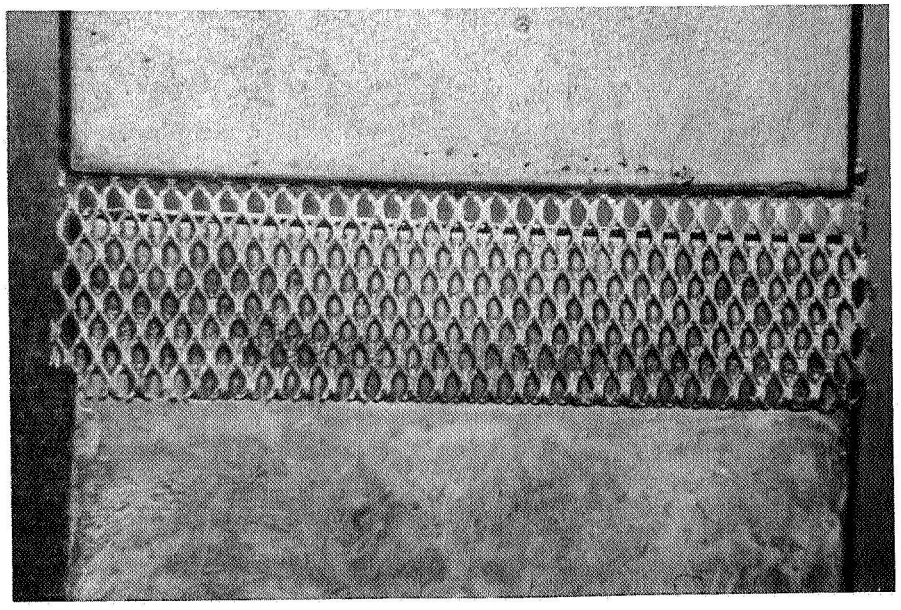

Figure 2-23. Closeup of Silver Mesh Interconnection (Back Side of Cell View)

A summary of test results is included as Table 2-8.

Table 2-8. Summary of Cell Test Results

Module	No. Cycles 1	Temperature Range	Test Results
1. CENTRALAB - 5S x 4P 8 Mil Cells Photoetched BeCu Interconnection (Solder Plated) "No Cover Slide"	100	+200°F (93.3°C) -200°F (-129°C)	10 of 20 Cells were Cracked 5 Cases of Solder Plating separation from Interconnection (No Post Test Performance Test possible due to Cell breakage)
2. JPL 8 Mil Cells - 5S x 5P 5/0 Silver Mesh Interconnection "No Cover Slide"	100	+200°F (93.3°C) -200°F (-129°C)	6 of 25 Cells were Cracked I_{sc} drop from 628 ma to 495 ma (133 ma Diff) I_{2v} drop from 601 ma to 431 ma (170 ma Diff) Severe Rounding of I-V "Knee"
3. JPL 8 Mil Cells - 5S x 5P 5/0 Silver Mesh Interconnection "6 Mil Cover Slide"	104	+200°F (93.3°C) +200°F (-129°C)	Satisfactory Test I_{sc} drop from 605 ma to 593 ma (2%) likely Test variation I-V Curve Shapes Identical No Interconnection Faults Detected
	100	+200°F (93.3°C) -210°F (-134.4°C)	Satisfactory Test I_{sc} held at 593 & 600 ma on Post Test Performance Curves I-V Curve Shapes Identical No Interconnection Faults Detected
	100	+200°F (93.3°C) -220°F (-140.0°C)	Satisfactory Test I_{sc} held at 588 & 596 ma on Post Test Performance Curves 4 ma Softening of Knee at 1.95V Indicates very slight increase in Series Resistance No Interconnection Faults Detected
	107	+200°F (93.3°C) -230°F (-145.6°C)	Satisfactory Test I_{sc} held at 592 & 593 ma on Post Test Performance Curves 5 ma Softening of Knee at 1.80V Indicates progressive increase in Series Resistance No Interconnection Faults Detected
	100	+200°F (93.3°C) -240°F (-151.1°C)	Failure Criteria Exceeded Negative Contact Cracked Across One Cell With Severe Softening of Knee (17 ma at 1.8V) resulting (I_{sc} only dropped to 585 ma)

2.3.4.6 Solar Panel Actuator

The SPAR Aerospace BI-STEM deployable boom was selected as the best technical approach during the Feasibility Study and remains the preferred approach for the solar panel actuator. Activities involving the completion of detailed specifications were carried out as the necessary prerequisites to the procurement of this item.

The general performance requirements, taken from the component specification, are given in Table 2-9. The solar panel actuator in the RA 250 design is a bolt-on component so that any deployable boom meeting the general performance requirements can be used with a minimum of design changes.

Table 2-9. General Performance Requirements for Solar Panel Actuator

Component Weight	12.0 pounds
Entended Length	33.5 ft $\pm$ 2 inches
Extension and Retraction Rate	1.5 inches per second $\pm$ 1 inch per second
Life	150 deploy/retract cycles Operate without malfunction after one year of interplanetary space environment
Loading Conditions	For vertical deployment in Earth's gravity field point: 4.0 pounds directed toward boom exit/from deployer mechanism 1.2 pounds of tip mass For deployment in space environment: 4.0 pounds directed toward boom exit point from deployer with solar flux of 260 mw/cm^2 incident on one-half of the boom while the other half is exposed to cold, black space Steady State space conditions: The boom shall not deflect laterally further than 50 inches at the tip in the fully extended position when subjected to a 4.0 pound force applied at the tip and directed toward the boom exit point from the deployment mechanism and when exposed to 260 mw/cm^2 of solar flux incident on one-half of the boom while the other half is exposed to cold, black space
Boom Straightness	When the boom is deployed vertically upward in the earth's gravitational field, the path of the boom tip shall remain within an 18-inch diameter circle centered on the nominal deployment axis.
Temperature Range	-130 deg C (-202 deg F) to 140 deg C (283 deg F)
Vibration and Shock	See Section 2.3.1

The BI-STEM unit will utilize a boom with a nominal outside diameter of 1.34 inches made of 301 stainless steel, silver plated on its outside surface. The boom is made up of two overlapping strips each a nominal four inches wide and 0.007 inche thick. The configuration of the BI-STEM boom is shown in Figure 2-24.

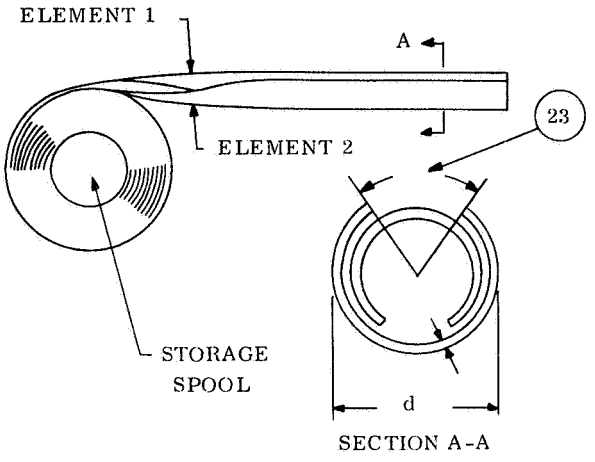

Figure 2-24. The BI-STEM Principle

2.3.4.7 Slip Ring Assembly

Activities prerequisite to placing an order for the slip ring assemblies have been carried out and vendor proposals have been solicited. Selected design parameters from the component specification are shown in Table 2-10.

2.3.5 DETAIL DESIGN

Detail design definition of the system elements is being developed and the drawings listed in Table 2-11 are being prepared. Because no assembly is completely defined at this time, no detail drawings have been included in this report.

The electrical system schematic is shown in Figure 2-25.

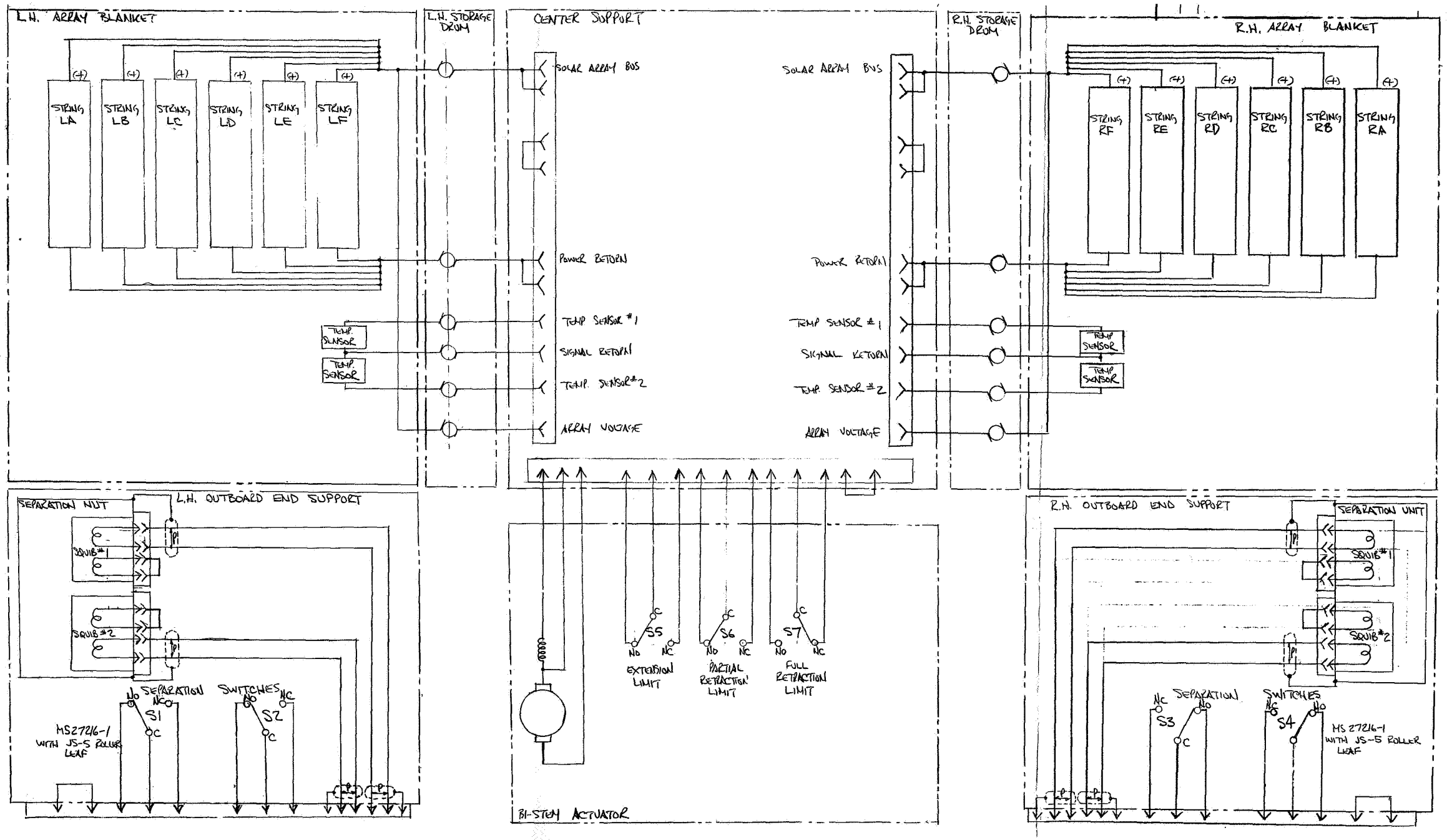

NOTE: ALL SWITCHES SHOWN WITH THE ARRAY FULLY RETRACTED AND THE OUTBOARD END SUPPORTS IN THE LAUNCH STOWED POSITION

Figure 2-25. Schematic of Electrical System for 30 Watts Per Pound Rollup Array

Table 2-10. Slip Ring Design Parameters

Power Rings per Assembly	2
Signal Rings per Assembly	4
Ring Material	Silver
Ring Diameter	0.75 in.
Brushes per Ring	2
Brush Material	Silver/Copper/ Niobium Diselenide/Graphite
Rated Current per Ring	
Power	15.0 amp dc
Signal	1.0 amp dc
Brush Contact Force	
Power	0.75 lb
Signal	0.10 lb
Starting Torque	
Air	0.7 in-lb
Vacuum	0.4 in-lb
Static Contact Resistance	0.005 ohms
Rated Current Density	
Power	75 Amp/in.^{2}
Signal	55 Amp/in.^{2}
Power Dissipation/assembly	1.53 watts
Weight/Assembly	0.50 lb

2.3.6 WEIGHT STATUS

The weight status of the RA250 system is shown in Table 2-12. Studies are underway to determine the effects of the present vibration loads on the weights of the structural elements and to minimize weight growth. A preliminary estimate of the structural weight increase is 3.0 pounds. Items which are affected to the largest extent are the center support, the end support brackets, and the drum support parts. The estimated weight increment is roughly divided between the three areas, but because detail design modifications have not been completed these increases have not been incorporated into Table 2-12.

The weight allowance for the BI-STEM assembly has been increased one pound in this present weight status report in accordance with the latest vendor information.

Table 2-11. RA 250 Drawing Tree

```
00010 *
00020 * DWG. TREE REVISION 3 (5/22/69)
00030 *
00040 * RA 250 ROLL-UP SOLAR SUBARRAY CONFIGURATION
00050 * 1.0  47J214519 ROLL-UP SOLAR ARRAY ASSEMBLY
00060 * 1.0.1    47E218199 ELECTRICAL SCHEMATIC,30W/# SYST.
00070 *
00080 * 1.1.0  47J214517 ARRAY BLANKET ASSEMBLY
00090 * 1.1.1    47E217892 SUBSTRATE-BUSBAR SHEET
00100 * 1.1.2    47E218181 MODULE, SOLAR CELL,19X20
00110 * 1.1.2.1    47C218185 SOLAR CELL,2 OHM-CM,8MIL
00120 * 1.1.2.2    47C218186 COVER SLIDE,FILTERED,3MIL
00130 * 1.1.2.3    47C218187 INTERCONNECTION, CELL TO CELL
00140 * 1.1.3    47C218188 INTERCONNECTION,MOD TO MOD
00150 *
00160 * 1.2.0  47E214524 BOOM ACTUATOR (REF. SVS 7552)
00170 * 1.2.1    47D214680 G3&G4 SADDLE BRACKET,LDG EDGE(ENG.MODEL)
00180 * 1.2.2    --------- CONNECTOR
00190 *
00200 * 1.3.0  --------- DRUM ASSEMBLY
00210 * 1.3.1    47E218194 DRUM SHELL
00220 * 1.3.2    --------- INBOARD END CAP ASSEMBLY
00230 * 1.3.2.1    --------- INBOARD END CAP
00240 * 1.3.2.2    --------- SUPPORT SHAFT
00250 * 1.3.2.3    --------- BEARING, BALL (SOURCE CONT.)
00260 * 1.3.2.4    --------- BRG. SPACER, OUTER RACE
00270 * 1.3.2.5    --------- BRG. SPACER, INNER RACE
00280 * 1.3.2.6    --------- BRG.RETAINER
00290 *
00300 *
```

* * * *

Table 2-11. RA250 Drawing Tree (Cont'd)

```
00310 *
00320 * 1.3.2.7    47B214689 SLIP RING ASSEMBLY(SVS 7547)
00330 * 1.3.2.8    --------- NEGATOR SPRING (SOURCE CONT.)
00340 * 1.3.2.9    --------- OUTPUT SPOOL NEGATOR
00350 * 1.3.2.10   --------- TAKE UP SPOOL,NEGATOR
00360 * 1.3.2.11   --------- POWER FEED THROUGH
00370 * 1.3.2.12   --------- FEED THROUGH HARNESS
00380 * 1.3.2.13   --------- BRG,BALL,TAKE UP SPOOL,(SOURCE)
00390 * 1.3.2.14   --------- MOUNTING BOLT T.U. SPOOL
00400 * 1.3.2.15   --------- WASHER,T.U.SPOOL BOLT
00410 * 1.3.3     -47C214512 OUTBOARD END CAP
00420 *
00430 * 1.4.0  --------- CENTER SUPPORT
00440 *
00450 * 1.5.0  47E214883 BOOM END MECH (LDG.EDGE)
00460 * 1.5.1    --------- BOOM ATTACHMENT POST
00470 * 1.5.2    --------- BEARING,BALL (SOURCE CONT.)
00480 * 1.5.3    --------- BEARING RETAINER
00490 *
00500 * 1.6.0  --------- OUTBOARD SUPPORT ASSEMBLY
00510 * 1.6.1    --------- MOVABLE ARM ASSEMBLY
00520 * 1.6.2    --------- HINGE BRACKET
00530 * 1.6.3    --------- TORSION SPRING
00540 * 1.6.4    --------- HINGE BOLT
00550 * 1.6.5    --------- MICROSWITCH ASSEMBLY
00560 * 1.6.6    47C218327 SEPARATION NUT (SOURCE CONT)
00570 * 1.6.7    --------- ELECTRICAL HARNESS
00580 * 1.6.8    --------- TAPERED PLUG, DRUM SUPPORT
00590 *
00600 *
                          * * * *
00610 *
00620 * 1.6.9    --------- TAPERED PLUG, LDG.EDGE SUPPORT
00630 * 1.6.10   47B218330 CARTRIDGE,PYROTECHNIC (SOURCE)
00640 * 1.6.11   47C218329 BOLT CATCHER (SOURCE CONT)
00650 * END
END OF FILE RA250
```

Table 2-12. Weight Status of RA 250 System

ITEM	PIECE	SUBASSEM.	COMPONENT	RA250
COMPLETE 250 SQ.FT. ROLL-UP SUBARRAY (31.986 W/@)				78.16 #
ARRAY BLANKET ASSEMBLY			42.04 #	
SUBST-BUSBAR BLANKET		7.37		
KAPTON	4.14			
BUTTONS	1.50			
BUS STRIP	1.20			
BUS ADHESIVE	0.53			
SOLAR CELL MODULES		34.67		
SOLAR CELLS	20.68			
COVER SLIDES	7.91			
COV.SLD.ADHESIVE	0.98			
INTERCONNECTIONS	2.04			
MOD-MOD INTERCON.	0.87			
SOLDER	0.19			
MOD BOND ADHESIVE	2.00			
BOOM ACTUATOR ASSEMBLY			12.17 #	
SPAR BI-STEM ASSEMBLY		12.00 #		
LDG.EDGE.SADDLE BRACKETS		0.08		
CONNECTOR		0.09		
DRUM ASSEMBLIES			16.11 #	
DRUM SHELLS		5.60		
* * * *				
INBOARD END CAP ASSEMBLIES		9.61		
INBOARD END CAPS	2.20			
SUPPORT SHAFTS	2.50			
BEARINGS,BALL	1.00			
BRG.SPACER,OUTER	0.18			
BRG.SPACER,INNER	0.15			
SLIP RING ASSEM'S	1.00			
NEGATOR SPRINGS	1.05			
NEG.OUTPUT SPOOLS	0.44			
NEG.TAKE-UP SPOOLS	0.14			
MTG.BOLT,T.U.SPL.	0.06			
POWER FEED THRUS	0.20			
HARNESS,FEED THRU	0.54			
THERMAL COATING		0.10		
OUTBOARD END CAP		0.80		
CENTER SUPPORT			1.70 #	
LEADING EDGE ASSEMBLY			1.00	
LEADING EDGE STRUCT.		0.80		
BEARINGS,BALL		0.10		
BRG.ADAPTER-RETAINER		0.10		
OUTBOARD SUPPORT ASSEMBLIES			5.14 #	
MOVABLE ARM ASSEMS.		2.9		
HINGE BRACKETS		0.6		
SPRINGS		0.3		
* * * *				
HINGE BOLTS		0.3		
SEPARATION NUTS		0.41		
PYROTECHNIC CARTRIDGES		0.13		
MICROSWITCHES		0.10		
INTERLOCK-FIRING HARNESS		0.40		

2.3.7 DEPLOYED DYNAMICS ANALYSIS

In any spacecraft application, the dynamics of an appendage the size of the RA250 are likely to be an important factor in the overall vehicle dynamics and operation of the overall vehicle dynamics and operation of the attitude control system. A combined analytical/ experimental study of the dynamic characteristics of the RA250 will be carried out in this project. The end product will be an experimentally verified analytical model which can be used to predict the performance of the RA250 and other rollup solar arrays.

During the Feasibility Study, an analytical model based on a stretched string model of the solar array blankets was used to calculate the lowest natural frequencies and associated mode shapes of the systems. Dr. R. Ross of JPL has significantly extended this model with a mesh representation of the solar array blankets. His studies indicate the lowest natural frequency is above 0.04 Hz. Additional analysis will be carried out with this finite element approach.

Most structural elements of the RA250 can be modeled adequately by the techniques commonly used to represent tubes, beams, and columns. However, the solar array blankets, which are a major system element, are unconventional structural elements and deserve special attention. A study of the solar array blankets is underway and the results reported in the following paragraphs have been achieved.

The principles of minimum potential energy and Hamilton's principle were first applied to determine the natural boundary conditions. The coordinates x, y and z were chosen in the direction of the length of the subpanel, in the direction of the width and in the transverse direction. The corresponding displacements are u, v and w. Further, the displacements and forces are divided into the equilibrium state (superscript 0) and the vibration state (superscript 1).

The non-linear strain displacement relationships are given by:

$$\epsilon_x = \frac{\partial u^0}{\partial x} + \frac{\partial u^1}{\partial x} + \frac{1}{2}\left(\frac{\partial w^1}{\partial x}\right)^2$$

$$\epsilon_y = \frac{\partial v^0}{\partial y} + \frac{\partial v^1}{\partial y} + \frac{1}{2}\left(\frac{\partial w^1}{\partial y}\right)^2 \qquad (2\text{-}1)$$

$$\gamma_{xy} = \frac{\partial u^0}{\partial y} + \frac{\partial v^0}{\partial x} + \frac{\partial u^1}{\partial y} + \frac{\partial v^1}{\partial x} + \left(\frac{\partial w^1}{\partial x}\right)\left(\frac{\partial w^1}{\partial y}\right)$$

The force-strain relationship is assumed to be linear and of the following form

$$N_x = E^*\left[(\epsilon_x^0 + \epsilon_x^1) + \nu^*(\epsilon_y^0 + \epsilon_y^1)\right]$$

$$N_y = E^*\left[(\epsilon_y^0 + \epsilon_y^1) + \nu^*(\epsilon_x^0 + \epsilon_x^1)\right] \qquad (2\text{-}2)$$

$$N_{xy} = \frac{E^*}{2}(1 - \nu^*)\left[\gamma_{xy}^0 + \gamma_{xy}^1\right]$$

where E* is the effective modulus relating force to strain and ν^* is the effective Poisson's ratio.

Applying the principles of minimum potential energy and variational calculus, and using equations (2-1) and (2-2) for the equilibrium state yields the following natural boundary conditions:

on $x = \pm a$

$$\frac{\partial u^0}{\partial x} + \nu^* \frac{\partial v^0}{\partial y} = \frac{N_x^0}{E^*} \qquad \text{or} \qquad \delta(u^0) = 0 \qquad (2\text{-}3)$$

$$\frac{\partial u^0}{\partial y} + \frac{\partial v^0}{\partial x} = \frac{2N_{xy}^0}{(1-\nu^*)E^*} \qquad \text{or} \qquad \delta(v^0) = 0$$

on $y = \pm b$

$$\nu^* \frac{\partial u^0}{\partial x} + \frac{\partial v^0}{\partial y} = \frac{N_y^0}{E^*} \qquad \text{or} \quad \delta(v^0) = 0$$

$$\frac{\partial u^0}{\partial y} + \frac{\partial v^0}{\partial x} = \frac{2N_{xy}^0}{(1-\nu^*)E^*} \qquad \text{or} \quad \delta(u^0) = 0 \tag{2-4}$$

Applying Hamilton's principle and variational calculus, and using the above results, yields the following natural boundary conditions for the vibration state:

on $x = \pm a$

$$\left[\frac{\partial u^1}{\partial x} + \frac{1}{2}\left(\frac{\partial w^1}{\partial x}\right)^2\right] + \nu^*\left[\frac{\partial v^1}{\partial y} + \frac{1}{2}\left(\frac{\partial w^1}{\partial y}\right)^2\right] = \frac{N_x^1}{E^*} \tag{2-5}$$

or $\delta(u^1) = 0$

$$\left[\frac{\partial u^1}{\partial y} + \frac{\partial v^1}{\partial x} + \left(\frac{\partial w^1}{\partial x}\right)\left(\frac{\partial w^1}{\partial y}\right)\right] = \frac{2N_{xy}^1}{(1-\nu^*)E^*}$$

or $\delta(v^1) = 0$

on $y = \pm b$

$$\nu^*\left[\frac{\partial u^1}{\partial x} + \frac{1}{2}\left(\frac{\partial w^1}{\partial x}\right)^2\right] + \left[\frac{\partial v^1}{\partial y} + \frac{1}{2}\left(\frac{\partial w^1}{\partial y}\right)^2\right] = \frac{N_y^1}{E^*}$$

or $\delta(v^1) = 0$

$$\left[\frac{\partial u^1}{\partial y} + \frac{\partial v^1}{\partial x} + \left(\frac{\partial w^1}{\partial x}\right)\left(\frac{\partial w^1}{\partial y}\right)\right] = \frac{2N_{xy}^1}{(1-\nu^*)E^*} \tag{2-6}$$

or $\delta(u^1) = 0$

The third boundary condition on both boundaries is automatically satisfied if both membrane forces are specified, since only two forces are possible. If both forces are not specified, then w^1 must be given. w^1 must be such as to eliminate rigid body motions. A brief discussion of these boundary conditions was given by Novozhilov [9]. These expressions can also be found by reducing the expressions obtained for sandwich plates by Yu [10] in the manner described by Goldenveizer [11]. The same results are obtained.

Due to the difficulty of determining the exact force distribution at the ends attached to the bar and the length of the subpanels, it is felt that the Rayleigh-Ritz method will yield the best results (Yu [12]). For the equilibrium state assume

$$u^0 = \sum_{i=1}^{J} a_i^0 \, u_i^0 \, (x, y)$$

$$v^o = \sum_{i=1}^{K} b_i^0 \, v_i^0 \, (x, y) \qquad (2\text{-}7)$$

where u_i^0 (x,y) and v_i^0 (x,y) are functions which satisfy the appropriate boundary conditions.

Thus, from the principle of minimum potential energy and the Rayleigh-Ritz method:

$$a_m^0 I_{mm}^1 + \sum_i^J \delta_{mi} a_i^0 I_{im}^1 + \sum_i^K b_i^0 I_{mi}^2 = \frac{2bW^*}{E^*} I_m^4$$

$$\text{for } m = 1, \; K \qquad (2\text{-}8)$$

$$b_m^0 I_{mm}^3 + \sum_i^K \delta_{mi} b_i^0 I_{im}^3 + \sum_i^J a_i^0 I_{im}^2 = 0$$

where W* is the weight per unit area, δ_{ij} is the kronecker delta ($\delta_{ij} = 0$ if $i = j$ and $\delta_{ij} = 1$ if $i = j$). The I_{ij}'s are a series of integrals of the functions u_i^0 and v_i^0. If these functions are chosen as orthogonal functions, equation (2-8) can be further simplified.

Similarly, for the vibration state, assume

$$u^1 = \sum_{i=1}^{L} a_i^1 u^1(x,y) e^{i\omega t}$$

$$v^1 = \sum_{i=1}^{M} b_i^1 v^1(x,y) e^{i\omega t} \qquad (2\text{-}9)$$

$$w^1 = \sum_{i=1}^{N} c_i^1 w^1(x,y) e^{i\omega t}$$

An application of Hamilton's principle and the Rayleigh-Ritz method leads to the following linearized equations

for m = 1, L

$$\left[a_m^1 I_{mm}^5 + \sum_i^L \delta_{mi} a_i^1 I_{im}^5 + \sum_i^M b_i^1 I_{mj}^6 \right] \frac{(e^{4\pi i} - 1)}{2}$$

$$+ \left[I_m^9 + \frac{1}{2} I_m^{11} \right] (e^{2\pi i} - 1) - \frac{2bW^*}{E^*} I_m^8 (e^{2\pi i} - 1)$$

$$+ \frac{\rho^* \omega^2}{E^*} \left[a_m^1 I_{mm}^{16} + \sum_i^L \delta_{mi} a_i^1 I_{im}^{16} \right] (e^{4\pi i} - 1)$$

$$= 0$$

for m = 1, M

$$\left[b_m^1 I_{mm}^7 + \sum_i^M \delta_{im} b_i^1 I_{im}^7 + \sum_i^L a_i^1 I_{im}^6 \right] \frac{(e^{4\pi i} - 1)}{2}$$

$$+ \left[I_m^{10} + \frac{1}{2} I_m^8 \right] (e^{2\pi i} - 1) + \frac{\rho^* \omega^2}{E^*} \left[b_m^1 I_{mm}^{17} \right.$$

$$\left. + \sum_i^M \delta_{im} b_i^1 I_{im}^{17} \right] (e^{4\pi i} - 1) = 0$$

for m = 1, N

$$\left[2c_m^1 \left(I_{mm}^{13} + I_{mm}^{14} + \frac{1}{4} I_{mm}^{15} + \sum_i^N \delta_{im} c_i^1 \left(2I_{im}^9 + 2I_{im}^{15} + \frac{1}{4}\left(I_{im}^{15} + I_{mi}^{15}\right)\right)\right)\right] \frac{\left(e^{4\pi i} - 1\right)}{2}$$

$$+ \frac{\rho^* \omega^2}{E^*} \left[c_m^1 I_{mm}^{18} + \sum_{i=1}^N \delta_{im} c_i^1 I_{im}^{18}\right] \left(e^{4\pi i} - 1\right) = 0 \qquad (2\text{-}10)$$

Again, these expressions can be simplified by the careful choice of orthogonal functions to represent the displacements.

Equations (2-8) and (2-10), along with the expressions for the various integrals involved, can be solved for the various modal frequencies and relative amplitudes. Both the gravity and zero gravity cases are included (for zero gravity W* = 0).

Work this quarter included the determination of appropriate coordinate functions for sub-situation into the integrals defined by equations (2-8) and (2-10). The following boundary conditions from the general set given in Equations 2-3, 2-4, 2-5, and 2-6 apply to the solar array blankets.

For the equilibrium state on $x = \pm a$;

$$v^\circ = 0$$

$$\frac{\partial u^\circ}{\partial x} + \nu^* \frac{\partial v^\circ}{\partial y} = \frac{N_x^\circ}{E^*} \qquad (2\text{-}11)$$

on $y = \pm b$;

$$\nu^* \frac{\partial u^\circ}{\partial x} + \frac{\partial v^\circ}{\partial y} = 0 \quad ,$$

$$\frac{\partial u^\circ}{\partial y} + \frac{\partial v^\circ}{\partial x} = 0 \tag{2-12}$$

For the perturbed state, on $x = \pm a$;

$$v^1 = 0 \quad ,$$

$$\int_{y=b}^{y=-b} \left\{ \left[\frac{\partial u^1}{\partial x} + \frac{1}{2}\left(\frac{\partial w^1}{\partial x}\right)^2 \right] + \nu^* \left[\frac{\partial v^1}{\partial y} + \frac{1}{2}\left(\frac{\partial w^1}{\partial y}\right)^2 - \frac{N_x^1}{E^*} \right] \right\} dy = 0 \tag{2-13}$$

on $y = \pm b$;

$$\int_{x=-a}^{x=a} \left\{ \left[\frac{\partial v^1}{\partial y} + \frac{1}{2}\left(\frac{\partial w^1}{\partial y}\right)^2 \right] + \nu^* \left[\frac{\partial u^1}{\partial x} + \frac{1}{2}\left(\frac{\partial w^1}{\partial x}\right)^2 \right] \right\} dx = 0$$

$$\int_{x=-a}^{x=a} \left\{ \left[\frac{\partial u^1}{\partial y} + \frac{\partial w^1}{\partial y} \right] + \left[\frac{\partial v^1}{\partial x} + \frac{\partial w^1}{\partial x} \right] \right\} dx = 0 \tag{2-14}$$

If applied in the integral form, i.e., integrand not equal to zero, the perturbed boundary conditions have been relaxed in that they are satisfied on the average rather than at every point along the boundary.

Because of the difficulty of finding functions whose zeroth and first order derivations are both zero on a given boundary, it is very difficult to select functions which are orthogonal. Thus, it was decided to compromise and use the method of Lagrange multipliers to satisfy the remaining boundary conditions. On this basis, the following functions were selected for the equilibrium solution:

$$u^o = a_o^o + \sum_{i=1}^{J_o} a_i^o \left[x \cos \frac{(2i-1)\pi y}{2b} \right]$$

$$v^o = \sum_{i=1}^{K_o} b_i^o \left[y \cos \frac{(2i-1)\pi x}{2a} \right] \qquad (2\text{-}15)$$

with the following auxilliary conditions:

$$\sum_{i=1}^{J_o} \frac{4ba_i^o (-1)^i}{(2i-1)\pi} + \int_{y=-b}^{y=b} \frac{N_x^o}{E^*} dy = 0 \qquad (2\text{-}16)$$

$$\sum_{i=1}^{K_o} \frac{4ab_i^o (-1)^i}{(2i-1)\pi} = 0$$

For the perturbed state:

$$u^1 = \sum_{i=1}^{J_o} a_i^1 \; x \cos \frac{(2i-1)\pi y}{2b} \; e^{i\omega t} \qquad (2\text{-}17)$$

$$v^1 = \sum_{i=1}^{K_o} b_i^1 \; y \cos \frac{(2i-1)\pi x}{2a} \; e^{i\omega t} \quad ,$$

$$w^1 = \sum_{i=1}^{L_o} c_i^1 \sin \frac{(2i-1)\pi x}{2a} \sin \frac{(2i-1)\pi y}{2b} \; e^{i\omega t} \quad ,$$

with the following auxilliary conditions;

$$\sum_{i=1}^{J_o} \frac{4ba_i^1(-1)^i}{(2i-1)\pi} + \int_{y=-b}^{y=b} \frac{N_x^1}{E^*}\,dy = 0 \quad ,$$

$$\sum_{i=1}^{K_o} \frac{4ab_i^1(-1)^i}{(2i-1)\pi} = 0 \quad , \tag{2-18}$$

$$\sum_{i=1}^{L_o} c_i^1 = 0$$

Note that this last relationship implies that w^1 is zero for the four corners. The method of Lagrange multipliers is a technique for solving a set of equations resulting from a minimization process. Define a new function:

$$F = f + \ell_1 g_1 + \ldots\ldots \ell_n g_n \tag{2-19}$$

where f is the original function to be minimized, g_n are the auxillary functions, and ℓ_n are the arbitrary multipliers. The function F is then minimized with respect to the original coefficients and the ℓ's, thus resulting in sufficient equations to solve for the coefficients and the multipliers.

For the equilibrium state, the following matrix equation can be written

$$\begin{bmatrix} & & \\ & A^o & \\ & & \end{bmatrix} \begin{bmatrix} a_o^o \\ a_i^o \\ \vdots \\ b_i^o \\ \vdots \\ \ell_1 \\ \ell_2 \end{bmatrix} = \begin{bmatrix} \\ B^o \\ \\ \end{bmatrix} \tag{2-20}$$

where A^o and B^o are matrices in terms of integrals of the coordinate functions. These can be partitioned into a more convenient form. A similar set of equations can be formed for the perturbed state.

$$\begin{bmatrix} & & \\ & A^1 & \\ & & \end{bmatrix} \begin{bmatrix} a_i^1 \\ \vdots \\ b_i^1 \\ \vdots \\ c_i^1 \\ \vdots \\ \ell_1 \\ \ell_2 \\ \ell_3 \end{bmatrix} = \begin{bmatrix} & & \\ & B^1 & \\ & & \end{bmatrix} \tag{2-21}$$

Equation (2-20) is readily solvable to determine the coefficients which describe the equilibrium position. These coefficients can then be used to establish A^1.

A^1 is a function of the perturbed coordinate functions, the equilibrium position and the natural frequencies. The natural frequencies are determined by setting the determinant of A^1 to zero and solving the resulting polynomial or by sweeping out the lowest mode. Evaluation of the values of the integrals appearing in A^o, B^o, A^1 and B^1 is currently under way.

2.4 MANUFACTURING DEVELOPMENT

2.4.1 INTRODUCTION

Development of manufacturing processes unique to the RA 250 was initiated this quarter. Areas of activity include the soldering process, application of cushioning buttons on back of rollup array, and tooling concepts.

2.4.2 SOLDERING TECHNIQUES

Infrared heating has been selected for solar cell soldering and development of the process is underway. A prototype solder machine has been assembled and is in use to determine optimum solder schedules, holding fixtures, and other details (See Figure 2-26).

A method to deposit controlled amounts of soldering desired locations on the silver mesh interconnects is needed for a successful solder process. The selected approach is to plate the solder out of solution onto the mesh. This approach gives every indication of being very successful. A sample of a solder joint is shown in Figure 2-27.

2.4.3 INTERCONNECT FABRICATION

The forming of interconnecting strips from silver mesh has been successfully accomplished using a prototype tool. A production tool for this process has been designed.

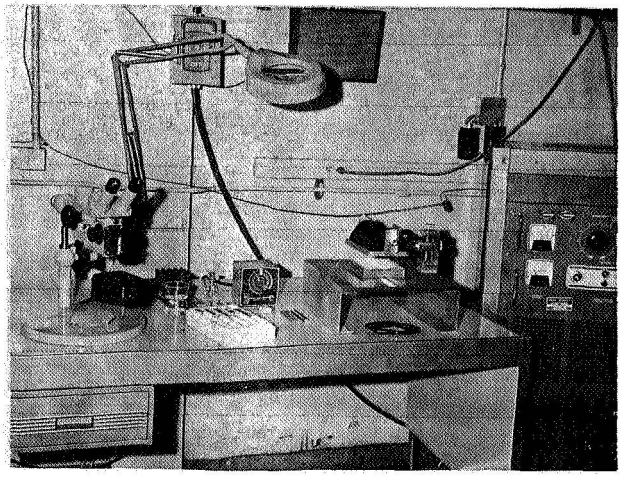

Figure 2-26. Prototype Infrared Soldering Machine

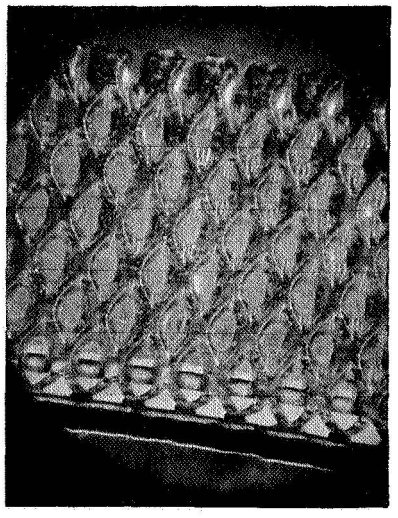

Figure 2-27. Silver Mesh Solder Joint Produced by Infrared Soldering Process

2.5 PLANS FOR NEXT PERIOD

The following activities are planned for the next period:

1. Complete the detail design and supporting analysis of the RA250 system and conduct a design review.

2. Generate the analytical modes for the dynamics of the stowed system, the dynamics of the deployed system, and the thermal characteristics of the system. These models will be used in test planning and the analysis of test results.

3. Initiate the design and fabrication of ground support equipment.

4. Initiate planning of the test program for the system

SECTION 3

CONCLUSIONS

The following conclusions have resulted from the first three months of effort on the design and development of the 30 watt per pound rollup subsolar array:

1. The change in environment levels from the Feasibility Study has a larger than anticipated impact on the detail design of the RA250 system.

2. In order to best accommodate the present launch environment, the structural design philosophy of the Feasibility Study should be modified to de-emphasize stiffness and introduce flexibility into the stowed configuration. This will lower the natural frequencies of the system and thereby reduce the dynamic loads resulting from the random vibration environment.

3. Though detailed studies have not been completed, the weight goal of 30 watts per pound is considered achievable for the present launch environment. The additional dynamic loads can be accommodated with a change in design.

4. Solar cell interconnections of expanded silver mesh have demonstrated adequacy with regard to the cold temperature extreme of the thermal environment and will be utilized in the RA250 design.

SECTION 4

RECOMMENDATIONS

There are no specific recommendations at this time. The project should continue at an accelerated pace during the next quarter, and detailed design information will be available in the next report.

SECTION 5

NEW TECHNOLOGY

No items of new technology have been identified or reported during this report period.

SECTION 6

REFERENCES

1. Final Report - Feasibility Study: 30 Watts per Pound Rollup Solar Array. 21 June 1968. Report No. 68SD4301, General Electric Company, Philadelphia, Pennsylvania.

2. Detail Specification for 30 Watts Per Pound Rollup Solar Cell Array. JPL Specification SS501407 Rev D. Approved for Release September 26, 1968.

3. Kirkpatrick, D. L., and Young, W. C., "Evaluation of Dry Lubricants and Bearings for Spacecraft Applications," General Electric Space Division, 3rd Aerospace Mechanisms Symposium, The Jet Propulsion Laboratory, May 23-24, 1968.

4. Clauss, Francis J., "Lubrication Evaluation," Materials Sciences Laboratory, Lockheed Missile and Space Co., April, 1966.

5. Clauss, Francis J., and Drake, Jr., Sanford P., "Vibration/Vacuum Screening of Space Lubricants," LMSC-684903, Final Report, Contract NAS 9-5114, National Aeronautics and Space Administration, Lockheed Missiles & Space Company, Sunnyvale, California, December 31, 1967.

6. Vest, C., and Ward, R., "Evaluation of Space Lubricants under Oscillatory and Slow Speed Rotary Motion," Goddard Space Flight Center, Lubrication Engineering, Vol. 24, No. 4, April, 1968, pp. 163-172.

7. Scibbe, Herbert W., Gleen, Dean C., and Anderson, William J., "Friction Torque of Ball Bearings in Vacuum with Seven Polytetrafluorethylene Composition Retainer Materials, NASA TN D-4355, Lewis Research Center, Cleveland, Ohio (Undated) Presented: September 1968.

8. Kirkpatrick, D. L., and Young, W. C., "Dry Lubricant Films are Now Practical for Many Rolling Element Bearings," General Electric Space Division, Machine Design, May 15, 1969.

9. Novozhilov, V. V., Thin Shell Theory; P. Noordhoff Ltd., 1964, pp. 109-111.

10. Yu, Y. Y., "Nonlinear Flexural Vibrations of Sandwich Plates," The Journal of the Acoustical Society of America, Vol. 34, No. 9, Part 1, Sept. 1962; pp. 1176-1183.

11. Goldenveizer, A. L., Theory of Elastic Thin Shells, Pergamon Press, 1961, pp. 110-121.

12. Yu, Y. Y., private communication.

GENERAL ELECTRIC

MISSILE AND SPACE DIVISION